

1 **SYNERGY BETWEEN SATELLITE OBSERVATIONS OF SOIL MOISTURE**  
2 **AND WATER STORAGE ANOMALIES FOR RUNOFF ESTIMATION**

3 Stefania Camici <sup>(1)</sup>, Gabriele Giuliani <sup>(1)</sup>, Luca Brocca <sup>(1)</sup>, Christian Massari <sup>(1)</sup>, Angelica Tarpanelli  
4 <sup>(1)</sup>, Hassan Hashemi Farahani <sup>(2)</sup>, Nico Sneeuw <sup>(2)</sup>, Marco Restano <sup>(3)</sup>, Jérôme Benveniste <sup>(4)</sup>

5 *(1) National Research Council, Research Institute for Geo-Hydrological Protection, Perugia, Italy ([s.camici@irpi.cnr.it](mailto:s.camici@irpi.cnr.it))*

6 *(2) Institute of Geodesy, University of Stuttgart, Geschwister-Scholl-Straße 24D, 70174 Stuttgart, Germany*

7 *(3) SERCO c/o ESA-ESRIN, Largo Galileo Galilei, Frascati, 00044, Italy*

8 *(4) European Space Agency, ESA-ESRIN, Largo Galileo Galilei, Frascati, 00044, Italy*

9

10

11

12

13

14

15

16

17

18

**November 2020**

19

Submitted to:

20

\* Correspondence to: Ph.D. Stefania Camici, Research Institute for Geo-Hydrological Protection, National Research Council, Via della Madonna Alta 126, 06128 Perugia, Italy. Tel: +39 0755014419 Fax: +39 0755014420 E-mail: [stefania.camici@irpi.cnr.it](mailto:stefania.camici@irpi.cnr.it).

## 21    **ABSTRACT**

22    This paper presents an innovative approach, STREAM - SaTellite based Runoff Evaluation And  
23    Mapping - to derive daily river discharge and runoff estimates from satellite soil moisture,  
24    precipitation and total water storage anomalies observations. Within a very simple model structure,  
25    precipitation and soil moisture data are used to estimate the *quick-flow* river discharge component  
26    while the total water storage anomalies are used for obtaining its complementary part, i.e., the *slow-*  
27    *flow* river discharge component. The two are then summed up to obtain river discharge estimates.  
28    The method is tested over the Mississippi river basin for the period 2003-2016 by using Tropical  
29    Rainfall Measuring Mission (TRMM) Multi-satellite Precipitation Analysis (TMPA) precipitation  
30    data, European Space Agency Climate Change Initiative (ESA CCI) soil moisture data and Gravity  
31    Recovery and Climate Experiment (GRACE) total water storage data. Despite the model simplicity,  
32    relatively high-performance scores are obtained in river discharge estimates, with a Kling-Gupta  
33    efficiency index greater than 0.64 both at the basin outlet and over several inner stations used for  
34    model calibration highlighting the high information content of satellite observations on surface  
35    processes. Potentially useful for multiple operational and scientific applications, from flood warning  
36    systems to the understanding of water cycle, the added-value of the STREAM approach is twofold:  
37    1) a simple modelling framework, potentially suitable for global runoff monitoring, at daily time scale  
38    when forced with satellite observations only, 2) increased knowledge on the natural processes, human  
39    activities and on their interactions on the land.

40

41    Key words: satellite products, soil moisture, water storage variations, conceptual hydrological  
42    modelling, rainfall-runoff modelling, Mississippi.

## 43 1. INTRODUCTION

44 Spatial and temporal continuous river discharge monitoring is paramount for improving the  
45 understanding of the hydrological cycle, for planning human activities related to water use as well as  
46 to prevent or mitigate the losses due to extreme flood events. To accomplish these tasks, runoff and  
47 river discharge data, which represents the aggregated signal of runoff (Fekete et al., 2012), should be  
48 available at adequate spatial and temporal resolution. For water resources management and drought  
49 monitoring monthly time series over basin area larger than 10'000 km<sup>2</sup> are sufficient whereas  
50 observations up to grid scale of few km and daily or sub-daily time step are required for flood  
51 prediction. The accurate spatio-temporally continuous runoff and river discharge estimation at finer  
52 spatial or temporal resolution is still a big challenge for hydrologists.

53 Traditional in situ observations of river discharge, even if generally characterized by high temporal  
54 resolution (up to sub-hourly time step), typically offer little information on the spatial distribution of  
55 runoff within a watershed. Moreover, river discharge observation networks suffer from many  
56 limitations such as low station density and often incomplete temporal coverage, substantial delay in  
57 data access and large decline in monitoring capacity (Vörösmarty et al., 2002). Paradoxically, this  
58 latter issue is exacerbated in developing nations (Crochemore et al., 2020), where the knowledge of  
59 the terrestrial water dynamics deserves greater attention due to huge damages to settlements and  
60 especially the loss of human lives that occurs regularly.

61 This precarious situation has led to growing interest in finding alternative solutions, i.e., model-based  
62 or observation-based approaches, for runoff and river discharge monitoring. Model-based  
63 approaches, based on the mathematical description of the main hydrological processes (e.g., water  
64 balance models, WBMs, global hydrological models, GHMs, e.g., Döll et al., 2003 or, increasing in  
65 complexity, land surface models, LSM, e.g., Balsamo et al., 2009; Schellekens et al., 2017), are able  
66 to provide comprehensive information on a large number of relevant variables of the hydrological  
67 cycle including runoff and river discharge at very high temporal and spatial resolution (up to hourly

sampling and 0.05° grid scale). However, the values of modelled water balance components rely on a massive parameterization of the soil, vegetation and land parameters, which is not always realistic, and are strongly dependent on the GHM or LSM models used, analysis periods ([Wisser et al., 2010](#)) and climate forcings selected (e.g. [Haddeland et al., 2012](#); [Gudmundsson et al., 2012a, b](#); [Prudhomme et al., 2014](#); [Müller Schmied et al., 2016](#)).

Alternatively, the observation-based approaches exploit machine learning techniques and a considerable amount of data to describe the physics of the system ([Solomatine and Ostfeld, 2008](#)) with only a limited number of assumptions. Besides being simpler than model-based approaches, these approaches still present some limitations. For example, they rely on a considerable amount of data describing the modelled system's physics and the spatial/temporal extent and the uncertainty of the resulting dataset is determined by both the spatial and temporal coverage and the accuracy of the forcing data (e.g., see E-RUN dataset, [Gudmundsson and Seneviratne, 2016](#); GRUN dataset, [Ghiggi et al., 2019](#); FLO1K dataset, [Barbarossa et al., 2018](#)). Additional limitations stem from the employed method to estimate runoff. Indeed, random forests such as employed in [Gudmundsson and Seneviratne \(2016\)](#) like other machine learning techniques, are powerful tools for data driven modeling, but they are prone to overfitting, implying that noise in the data can obscure possible signals ([Hastie et al., 2009](#)). Moreover, the influence of land parameters on continental-scale runoff dynamics is not considered as the underlying hypothesis is that the hydrological response of a basin exclusively depends on present and past atmospheric forcing. It is easy to understand that this assumption will only be valid in certain circumstances and might lead to problems, e.g., over complex terrain ([Orth and Seneviratne, 2015](#)) or in cases of human river flow regulation ([Ghiggi et al., 2019](#)).

Remote sensing can provide estimates of nearly all the climate variables of the global hydrological cycle including soil moisture (e.g., [Wagner et al., 2007](#); [Seneviratne et al., 2010](#)), precipitation ([Huffman et al., 2014](#)) and total terrestrial water storage (e.g., [Houborg et al., 2012](#); [Landerer and Swenson, 2012](#); [Famiglietti and Rodell, 2013](#)). It has undeniably changed and improved dramatically the ability to monitor the global water cycle and, hence, runoff. By taking advantage of satellite

94 information, some studies tried to develop methodologies able to optimally produce multivariable  
95 datasets from the fusion of in situ and satellite-based observations (e.g., Rodell et al., 2015; Zhang et  
96 al., 2018; Pellet et al., 2019). Other studies exploited satellite observations of hydrological variables,  
97 e.g., precipitation (Hong et al., 2007), soil moisture (Massari et al., 2014), and geodetic variables (e.g.,  
98 Sneeuw et al., 2014; Tourian et al., 2018) to monitor single components of the water cycle in an  
99 independent way.

100 Although the majority of these studies provide runoff and river discharge data at basin scale and  
101 monthly time step, they deserve to be recalled here as important for the purpose of the present study.  
102 In particular, Hong et al. (2007) presented a first attempt to obtain an approximate but quasi-global  
103 annual streamflow dataset by incorporating satellite precipitation data in a relatively simple rainfall-  
104 runoff simulation approach. Driven by the multiyear (1998-2006) Tropical Rainfall Measuring  
105 Mission Multi-satellite Precipitation Analysis, runoff was independently computed for each global  
106 land surface grid cell through the Natural Resources Conservation Service (NRCS) runoff curve  
107 number (CN) method (NRCS, 1986) and subsequently routed to the watershed outlet to predict  
108 streamflow. The results, compared to the in situ observed river discharge data, demonstrated the  
109 potential of using satellite precipitation data for diagnosing river discharge values both at global scale  
110 and for medium to large river basins. If, on the one hand, the work of Hong et al. (2007) can be  
111 considered as a pioneer study, on the other hand it presents a serious drawback within the NRCS-CN  
112 method that lacks a realistic definition of the soil moisture conditions of the catchment before flood  
113 events. This aspect is not negligible as it is well established that soil moisture is paramount in the  
114 partitioning of precipitation into surface runoff and infiltration inside a catchment (Brocca et al.,  
115 2008). In particular, for the same rainfall amount but different values of initial soil moisture  
116 conditions, different flooding effects can occur (see e.g. Crow et al., 2005; Brocca et al., 2008; Berthet  
117 et al., 2009; Merz and Blöschl, 2009; Tramblay et al., 2010). On this line following Brocca et al.  
118 (2009), Massari et al. (2016) presented a very first attempt to estimate global streamflow data by  
119 using satellite Soil Moisture Active and Passive (SMAP, Entekhabi et al., 2010) and Global

Precipitation Measurement (GPM, [Huffman et al., 2019](#)) products. Although the validation was carried out by routing the monthly surface runoff only in a single basin in Central Italy, the obtained results suggested to dedicate additional efforts in this direction.

Among the studies that use satellite observations of hydrological variables for runoff estimation, the hydro-geodetic approaches are undoubtedly worth mentioning, see e.g., [Sneeuw et al. \(2014\)](#) for a comprehensive overview or [Lorenz et al. \(2014\)](#) for an analysis of satellite-based water balance misclosures with discharge as closure term. In particular, the satellite mission Gravity Recovery And Climate Experiment (GRACE), which observed the temporal changes in the gravity field, has given a strong impetus to satellite-driven hydrology research ([Tapley et al., 2019](#)). Since temporal gravity field variations over the continents imply water storage change, GRACE was the first remote sensing system to provide observational access to deeper groundwater storage. GRACE and its successor mission GRACE-FO provide monthly snapshots of the Earth's gravity field. The temporal variation is therefore relative to the temporally mean gravity field and, hence, the time variations of water storage are fundamentally relative to the mean storage. This relative water storage variation is termed Total Water Storage Anomaly (TSWA).

The relation between GRACE-derived TWSA and runoff was characterized by [Riegger and Tourian \(2014\)](#), which even allowed the quantification of absolute drainable water storage over the Amazon ([Tourian et al., 2018](#)). In essence, the storage-runoff relation describes the gravity-driven drainage of a basin and, hence, the slow-flow processes. Due to GRACE's spatial-temporal resolution, runoff and river discharge are generally available for large basins ( $>160'000 \text{ km}^2$ ) and at monthly time step.

Based on the above discussion, it is clear that each approach presents strengths and limitations that enable or hamper the runoff and river discharge monitoring at finer spatial and temporal resolutions. In this context, this study presents an attempt to find an alternative method to derive daily river discharge and runoff estimates at  $0.25^\circ$  degree spatial resolution exploiting satellite observations and the knowledge of the key mechanisms and processes that act in the formation of runoff, i.e., the role of soil moisture in determining the response of a catchment to precipitation. For that, soil moisture,

precipitation and TWSA observations are used as input into a simple modelling framework named STREAM v1.3 (SaTellite based Runoff Evaluation And Mapping, version 1.3, hereafter referred to as STREAM). Unlike classical LSMs, STREAM exploits the knowledge of the system states (i.e., soil moisture and TWSA) to derive river discharge and runoff, and thus it 1) skips the modelling of the evapotranspiration fluxes which are known to be a non-negligible source of uncertainty (Long et al. 2014), 2) limits the uncertainty associated with the over-parameterization of soil and land parameters and 3) implicitly takes into account processes, mainly human-driven (e.g., irrigation, change in the land use), that might have a large impact on the hydrological cycle and hence on runoff. The detailed description of the STREAM model is given in paragraph 4. The collected datasets and the experimental design for the Mississippi River Basin (paragraph 2) are described in paragraph 3 and 5, respectively. Results, discussion and conclusions are drawn in paragraph 6, 7 and 8, respectively.

## 2. STUDY AREA

The STREAM model presented here has been tested and validated over the Mississippi River basin (Figure 1a). With a drainage area of about 3.3 million km<sup>2</sup>, the Mississippi River basin is the fourth largest watershed in the world, bordered to the West by the crest of the Rocky Mountains and to the East by the crest of the Appalachian Mountains. According to the Köppen climate classification, the climate is subtropical humid over the southern part of the basin, continental humid with hot summer over the central part, continental humid with warm summer over the eastern and northern parts, whereas a semiarid cold climate affects the western part. The average annual air temperature across the watershed ranges from 4°C in the West to 6°C in the East. On average, the watershed receives about 900 mm/year of precipitation (77% as rainfall and 23% as snowfall), more concentrated in the eastern and southern portions of the basin with respect to its northern and western part (Vose et al., 2014).

170 The river flow has a clear natural seasonality mainly controlled by spring snowmelt (coming from  
171 the Missouri and the Upper Mississippi, the eastern and the upper part of the basin, respectively, Dyer  
172 2008) and by heavy precipitation exceeding the soil moisture storage capacity (mostly occurring in  
173 the eastern and southern part of the basin, Berghuijs et al., 2016). The basin is also heavily regulated  
174 by the presence of large dams (Global Reservoir and Dam Database GRanD, Lehner et al., 2011)  
175 most of them located on the Missouri river, over the Great Plains. In particular, the river reach  
176 between Garrison and Gavins Point dams is the portion of the Missouri river where the large main-  
177 channel dams have the greatest impact on river discharge providing a substantial reduction in the  
178 annual peak floods, an increase on low flows and a reduction on the overall variability of intra-annual  
179 discharges (Alexander et al., 2012). The annual average of Mississippi river discharge at Vicksburg,  
180 the outlet river cross-section of the basin, is equal to 17'500 m<sup>3</sup>/s (see Table 1). Given the variety of  
181 climate and topography across the Mississippi River basin, it is a good candidate to test the suitability  
182 of the STREAM model for river discharge and runoff simulation.

### 183 **3. DATASETS**

184 The datasets used in this study include in situ observations, satellite products and runoff verification  
185 data. The first two datasets are used as input data to the STREAM model. Conversely, the runoff  
186 verification data are used as a benchmark to validate the performance of the STREAM model in  
187 simulating the runoff.

#### 188 **3.1 In situ Observations**

189 In situ observations comprise air temperature and river discharge data.

190 For air temperature data the Climate Prediction Center (CPC) Global Temperature data developed by  
191 the American National Oceanic and Atmospheric Administration (NOAA) using the optimal  
192 interpolation of quality-controlled gauge records of the Global Telecommunication System (GTS)  
193 network (Fan et al., 2008) have been used. The dataset is available on a global regular 0.5°×0.5° grid  
194 and provides daily maximum ( $T_{\max}$ ) and minimum ( $T_{\min}$ ) air temperature data from 1979 to present



195 (2022). The daily average air temperature data have been generated as the mean of  $T_{\max}$  and  $T_{\min}$  of  
196 each day.

197 Daily river discharge data over the study basin have been taken from the Global Runoff Data Center  
198 (GRDC, [https://www.bafg.de/GRDC/EN/Home/homepage\\_node.html](https://www.bafg.de/GRDC/EN/Home/homepage_node.html)). In particular, 11 gauging  
199 stations located along the main river network of the Mississippi River basin have been selected to  
200 represent the spatial distribution of river discharge over the basin. The location of these gauging  
201 stations along with relevant characteristics (e.g., the upstream basin area, the mean annual river  
202 discharge and the presence of upstream dams) are summarized in Table 1. Mean annual river  
203 discharge ranges from 141 to 17'500 m<sup>3</sup>/s, and 3 of 11 gages are located downstream of big dams  
204 ([Lehner et al., 2011](#)). In particular, gages 1, 2 and 5 are located downstream of Garrison (the fifth-  
205 largest earthen dam in the world), Gavins Point and Kanopolis dams, respectively (see Figure 1a and  
206 Table 1). The related reservoirs have a maximum storage of 29383×10<sup>9</sup> m<sup>3</sup>, 0.607×10<sup>9</sup> m<sup>3</sup>, and  
207 1.058×10<sup>9</sup> m<sup>3</sup>, respectively.

### 208 **3.2 Satellite Products**

209 Satellite products include observations of precipitation, soil moisture and TWSA.

210 The satellite precipitation dataset used in this study is the Multi-satellite Precipitation Analysis 3B42  
211 Version 7 (her after referred to as TMPA) estimate produced by the National Aeronautics and Space  
212 Administration (NASA) as the 0.25°×0.25° quasi-global (50°S-50°N) gridded dataset. The TMPA is  
213 a gauged-corrected satellite product, with a latency period of two months, available at 3h sampling  
214 interval from 1998 to present. Major details about the  $P$  dataset, downloadable from  
215 <http://pmm.nasa.gov/data-access/downloads/trmm>, can be found in [Huffman et al. \(2007\)](#).

216 Soil moisture data have been taken from the European Space Agency Climate Change Initiative (ESA  
217 CCI) Soil Moisture project (<https://esa-soilmoisture-cci.org/>) that provides a surface soil moisture  
218 product (referred to first 2–3 cm of soil) continuously updated in terms of spatial-temporal coverage,  
219 sensors and retrieval algorithms ([Dorigo et al., 2017](#)). In this study, the daily combined ESA CCI soil

220 moisture product v4.2 is used. It is available at global scale with a grid spacing of  $0.25^\circ$ , for the period  
221 1978 to present.

222 TWSA have been obtained from the Gravity Recovery And Climate Experiment (GRACE) satellite  
223 mission. Here we employ the NASA Goddard Space Flight Center (GSFC) global mascon model,  
224 i.e., Release v02.4, ([Luthcke et al. 2013](#)). It has been produced based on the mass concentration  
225 (mascon) approach. The model provides surface mass densities on a monthly basis. Each monthly  
226 solution represents the average of surface mass densities within the month, referenced at the middle  
227 of the corresponding month. The model has been developed directly from GRACE level-1b K-Band  
228 Ranging (KBR) data. It is computed and delivered as surface mass densities per patch over blocks of  
229 approximately  $1^\circ \times 1^\circ$  or about  $12'000 \text{ km}^2$ . Although the mascon size is smaller than the inherent  
230 spatial resolution of GRACE of about  $2.5^\circ \times 2.5^\circ$  or  $64'000 \text{ km}^2$  ([Vishwakarma et al., 2018](#)), the model  
231 exhibits a relatively high spatial resolution. This is attributed to a statistically optimal Wiener  
232 filtering, which uses signal and noise full covariance matrices. This allows the filter to fine tune the  
233 smoothing in line with the signal-to-noise ratio in different areas. That is, the less smoothing, the  
234 higher signal-to-noise ratio in a particular area and vice versa. This ensures that the filtering is  
235 minimal and aggressive smoothing is avoided when unnecessary. Further details of such a filter can  
236 be found in [Klees et al. \(2008\)](#). Importantly, the coloured noise characteristic of KBR data was taken  
237 in to account when compiling the GRACE model, which has allowed for a reliable computation of  
238 the aforementioned noise full covariance matrices. The coloured noise characteristic of KBR data  
239 was taken into account when compiling the model, which has allowed for a reliable computation of  
240 these noise and signal covariance matrices. They play a crucial role when filtering and allow a higher  
241 spatial resolution compared to commonly applied GRACE filtering methods such as Gaussian  
242 smoothing and/or destriping filters. The GRACE data used here are available from January 2003 to  
243 July 2016, which suffices to demonstrate the STREAM capabilities. With its successor mission  
244 GRACE Follow-On (GRACE-FO), launched early 2018, the time series of time-variable gravity has  
245 reached a nearly uninterrupted time span of about 20 years, thus allowing a continued and operational

246 use of STREAM. The existing interruptions, short ones due to mission operations or technical  
247 failures, but also the one-year gap between GRACE and GRACE-FO can be dealt with in various  
248 ways, e.g. by data driven gap filling (Yi and Sneeuw, 2021).

### 249 **3.3 Runoff Verification Data**

250 To establish the quality of the STREAM model in runoff simulation, monthly runoff data obtained  
251 from the Global Runoff Reconstruction (GRUN\_v1, <https://doi.org/10.3929/ethz-b-000324386>) have  
252 been used for comparison. The GRUN dataset (Ghiggi et al., 2019) is a global monthly runoff dataset  
253 derived through the use of a machine learning algorithm trained with in situ river discharge  
254 observations of relatively small catchments (<2500 km<sup>2</sup>) and gridded precipitation and temperature  
255 derived from the Global Soil Wetness Project Phase 3 (GSWP3) dataset (Kim et al., 2017). The  
256 dataset covers the period from 1902 to 2014 and it is provided on a 0.5° × 0.5° regular grid.

## 257 **4. METHOD**

### 258 **4.1 STREAM Model: the Concept**

259 The STREAM model conceives river discharge as a combination of hydrological responses operating  
260 at diverse time scales (Blöschl et al., 2013; Rakovec et al., 2016). In particular, river discharge can  
261 be considered made up of a *slow-flow* component, produced as outflow of the groundwater storage  
262 and of a *quick-flow* component, i.e. mainly related to the surface and shallow-subsurface runoff  
263 components (Hu and Li, 2018).

264 While the high spatial and temporal variability of precipitation and the highly changing land cover  
265 spatial distribution significantly impact the variability of the *quick-flow* river discharge component  
266 (with scales ranging from hours to days and metres to kilometres depending on the basin size), *slow-*  
267 *flow* river discharge reacts to precipitation inputs more slowly as water infiltrates, is stored, mixed  
268 and is eventually released in times spanning from weeks to months. Therefore, the two components  
269 can be estimated by relying upon two different approaches that involve different types of  
270 observations. Based on that, within the STREAM model, satellite soil moisture, precipitation and

271 TWSA will be used for deriving river discharge and runoff estimates. The first two variables are used  
272 as proxy of the *quick-flow* river discharge component while TWSA is exploited for obtaining its  
273 complementary part, i.e., the *slow-flow* river discharge component. Firstly, we exploit the role of the  
274 soil moisture in determining the response of the catchment to the precipitation inputs, which have  
275 been soundly demonstrated in more than ten years of literature studies (see e.g., [Brocca et al., 2017](#)  
276 for a comprehensive discussion on the topic). Secondly, we consider the important role of total water  
277 storage in determining the *slow-flow* river discharge component as modelled in several hydrological  
278 models (e.g., [Sneeuw et al., 2014](#)).

279 It is worth noting that modeling the *quick-flow* and *slow-flow* river discharge components  
280 independently has been largely applied and tested in recent and past studies, e.g., for the estimation  
281 of the flow duration curve (see e.g., [Botter et al., 2007a, b](#); [Yokoo and Sivapalan 2011](#); [Muneepeerakul](#)  
282 [et al., 2010](#); [Ghotbi et al., 2020](#)).

## 283 **4.2 STREAM Model**

284 The STREAM model is a semi-distributed conceptual hydrological model that uses gridded satellite-  
285 derived inputs of precipitation, soil moisture, TWSA and air temperature to estimate daily values of  
286 gridded runoff and river discharge time series at select basin outlets.

287 To set up the model, the catchment is divided into  $b$  sub-catchments, each one representing either a  
288 tributary draining area with outlet along the main channel or an area draining directly into the main  
289 channel (see Figure 2). Each sub-catchment, assumed homogeneous, is further divided into an array  
290  $N_b$  of individual cells assumed as the unit basis for the runoff generation. Note that the number  $N_b$   
291 differs for each sub-catchment as, for a fixed cell grid size, it varies with the sub-catchment area.  
292 Once estimated at cell scale and aggregated at the sub-basin scale (see paragraph 4.2.1 for details),  
293 the runoff is routed at each sub-catchment outlet (see paragraph 4.2.2) and then transferred through  
294 the channels and the rivers for the computation of the river discharge at intermediate outlets or at the  
295 outlet of the entire basin (see paragraph 4.2.3).

Based on that, hereinafter we refer to river discharge,  $Q$ , to indicate the amount of water passing a particular point of a river (in  $\text{m}^3 \text{s}^{-1}$ ) whereas runoff,  $R$ , is regarded as the depth of water produced from a drainage area during a particular time interval (in mm). The difference between the two quantities is related to the routing processes that allow to transform the runoff into river discharge.

#### 4.2.1 Runoff generation at cell scale

The soil zone of each cell  $i$  of the basin is divided into two layers, the upper and lower soil storages allowing to model the related runoff responses,  $R_{q,i}$  [mm] and  $R_{s,i}$  [mm], as illustrated in Figure 2b.

The upper cell storage receives inputs from precipitation ( $P_i$ ), released through a snow module (Cislaghi et al., 2020) as rainfall ( $r_i$ ) or stored as snow water equivalent ( $SWE_i$ ) within the snowpack and on the glaciers. In particular, according to Cislaghi et al. (2020),  $SWE_i$  is modelled by using as input air temperature ( $T_{\text{air},i}$ ) and a degree-day coefficient,  $C_m$ , to be estimated by calibration.

Once precipitation is partitioned by the snow model, the rainfall output  $r_i$  contributes to  $R_{q,i}$  while the  $SWE_i$  (like other fluxes contributing to modify the soil water content into  $Su$ ) is neglected as already considered in the satellite TWSA. Therefore, the first key point of the STREAM model is that the water content in the upper storage of soil zone,  $Su$  (Figure 2b), is directly provided by the satellite soil moisture observations and the loss processes like percolation or evaporation do not need to be explicitly modelled to estimate the evolution in time of soil moisture. Consequently, for each cell  $i$ ,  $R_{q,i}$  can be computed following the formulation proposed by Georgakakos and Baumer (1996), as in equation (1):

$$R_{q,i}(t) = r_i(t) SWI_i(t, T)^\alpha \quad (1)$$

where:

-  $t$  [days] represents the time;

-  $r_i$  [mm] is the rainfall, obtained as an output from the snow module;

319 -  $SWI_i$  [-] is the Soil Water Index (Wagner et al., 1999), i.e., the root-zone soil moisture product  
 320 referred to the first layer of the model (representative of the first 5–30 cm of soil), derived by the  
 321 surface satellite soil moisture product,  $\theta_i$ , by applying the exponential filtering approach in its  
 322 recursive formulation (Albergel et al., 2009):

$$323 \quad SWI_{i,n} = SWI_{i,n-1} + K_n(\theta_i(t_n) - SWI_{i,n-1}) \quad (2)$$

324 with the gain  $K_n$  at the time  $t_n$  given by:

$$325 \quad K_n = \frac{K_{n-1}}{K_{n-1} + e^{\left(\frac{t_n - t_{n-1}}{T}\right)}} \quad (3)$$

326 -  $T$  [days] is a parameter, named characteristic time length, that characterizes the temporal variation  
 327 of soil moisture within the root-zone profile and the gain  $K_n$  ranges between 0 and 1;

328 -  $\alpha$  [-] is a coefficient linked to the non-linearity of the infiltration process and it considers the  
 329 characteristics of the soil;

330 - for the initialization of the filter  $K_1 = 1$  and  $SWI_1 = \theta(t_1)$ .

331 The second key point of STREAM model concerns the estimation of  $R_{s,i}$ , i.e., the *slow-runoff* response  
 332 related to the lower storage of the soil zone. The hypothesis here, shared also with other studies (e.g.,  
 333 Rakovec et al., 2016), is that the dynamic of  $R_s$  can be represented by the monthly TWSA data. Indeed,  
 334 the time scale of  $R_s$  is typically in the range of seasons to years and it can be assumed almost  
 335 independent of the water that is contained in the upper storage. For that, for each cell  $i$ ,  $R_{s,i}$  can be  
 336 computed following the formulation proposed by Famiglietti and Wood (1994), through equation (4)  
 337 as follows:

$$338 \quad R_{s,i}(t) = \beta (TWSA_i^*(t))^m \quad (4)$$

339 where:

340 -  $TWSA_i^*$  [-] is the TWSA estimated by GRACE over the cell  $i$  normalized by its minimum and  
 341 maximum values. The assumption behind this equation is that TWSA can be assumed as a proxy  
 342 of the evolution in time of the  $Sl$ , i.e., the water amount in the lower storage of the soil zone.  
 343 -  $\beta$  [mm h<sup>-1</sup>] and  $m$  [-] are two parameters describing the nonlinearity between lower storage runoff  
 344 component and  $TWSA^*$ .

345 Note that we made the hypothesis that soil moisture and TWSA observations are independent  
 346 (whereas in reality soil moisture can be responsible both for the generation of  $R_q$  (mainly) and for the  
 347  $R_s$  contribution) given the different temporal (and spatial) scales at which the upper and lower runoff  
 348 responses act.

349 By neglecting any lateral flow, the runoff responses at cell scale are averaged at sub-catchment scale  
 350 to obtain  $b$  runoff responses, one for each sub-catchment. Specifically, by considering  $N_b$  cells for  
 351 each sub-catchment, the following equation are used:

$$352 \quad R_{q,b}(t) = \frac{\sum_{i=1}^{N_b} R_{q,i}(t)}{N_b} \quad (5)$$

$$353 \quad R_{s,b}(t) = \frac{\sum_{i=1}^{N_b} R_{s,i}(t)}{N_b} \quad (6)$$

#### 354 **4.2.2 Sub-catchment river discharge calculation**

355 For each sub-catchment  $b$ , the runoff component  $R_{q,b}$  is routed to its outlet by the Geomorphological  
 356 Instantaneous Unit Hydro-graph (GIUH, Gupta et al., 1980) for tributary draining areas or through a  
 357 linear reservoir approach (Nash, 1957) for directly draining areas. The  $R_{s,b}$  runoff component is  
 358 transferred to the sub-catchment outlet by a linear reservoir approach. These processes are controlled  
 359 by a parameter lag time,  $L$  [days], evaluated as (Corradini et al., 2002):

$$360 \quad L = \gamma 1.19 A_b^{0.33} \quad (7)$$

361 where  $A_b$  [km<sup>2</sup>] is the sub-catchment area and  $\gamma$  [-] is a parameter to be calibrated.

362 By routing the  $R_{q,b}$  and  $R_{s,b}$  components the *quick-flow*,  $Q_{q,b}$  [m<sup>3</sup>/s], and the *slow-flow*,  $Q_{s,b}$  [m<sup>3</sup>/s]  
363 river discharge components at each sub-catchment outlet are obtained (see Figure 2c).

#### 364 **4.2.3 River discharge routing through river networks**

365 A diffusive linear approach (controlled by the parameters  $C$  [km h<sup>-1</sup>] and  $D$  [km<sup>2</sup> h<sup>-1</sup>], i.e., Celerity  
366 and Diffusivity, Troutman and Karlinger, 1985) is applied to route the two river discharge  
367 components,  $Q_{q,b}$  and  $Q_{s,b}$  through the river network from the sub-catchment outlet to intermediate  
368 outlets along the river or to the outlet of the entire basin (Brocca et al., 2011). In this way the *quick-*  
369 *flow*,  $Q_q$  [m<sup>3</sup>/s], and the *slow-flow*,  $Q_s$  [m<sup>3</sup>/s] river discharge components at the catchment outlet are  
370 obtained (see Figure 2d).

#### 371 **4.3 STREAM Parameters**

372 The STREAM model uses 8 calibration parameters for each sub-catchment  $b$  into which the entire  
373 basin is divided. Among these parameters, 5 control the runoff generation process ( $\alpha$ ,  $T$ ,  $\beta$ ,  $m$ ,  $C_M$ )  
374 and 3 the routing component and therefore the streamflow dynamics ( $\gamma$ ,  $C$  and  $D$ ). The parameter  
375 values determined within the feasible parameter space (See Table Appendix A for more details), are  
376 calibrated by maximizing the Kling-Gupta Efficiency index (***KGE***, Gupta et al., 2009; Kling et al.,  
377 2012, see paragraph 5.1 for more details) between observed and modelled river discharge. For model  
378 calibration, a standard gradient-based automatic optimisation method (Bober 2013) was used.

### 379 **5. EXPERIMENTAL DESIGN**

#### 380 **5.1 Modelling Setup for Mississippi River Basin**

381 The modelling setup is carried out in three steps (Figure 3):

382 1. *Sub-catchment delineation*. The TopoToolbox (<https://topotoolbox.wordpress.com/>), a tool  
383 developed in Matlab by Schwanghart et al. (2010), and the SHuttle Elevation Derivatives at multiple  
384 Scales (HydroSHED, <https://www.hydrosheds.org/>) DEM of the basin at the 3'' resolution (nearly 90  
385 m at the equator) have been used to derive flow directions, to extract the stream network and to



delineate the drainage basins over the Mississippi River basin. In particular, by considering only rivers with order greater than 3 (according to the Horton-Strahler rules, Horton, 1945; Strahler, 1952), the Mississippi watershed has been divided into 53 sub-catchments as illustrated in Figure 1a. Blue lines in the figure illustrate the river network pathway connecting the sub-catchments, red dots indicate the location of the 11 river discharge gauging stations selected for the study area.

It has to be specified that the step of sub-basin delineation could be accomplished through tools different from the TopoToolbox. For instance, it could be used the free Qgis software downloadable at <https://www.qgis.org/it/site/forusers/download.html>, following the instruction to perform the hydrological analysis as in [https://docs.qgis.org/3.16/en/docs/training\\_manual/processing/hydro.html?highlight=hydrological%20analysis](https://docs.qgis.org/3.16/en/docs/training_manual/processing/hydro.html?highlight=hydrological%20analysis).

*2. Extraction of input data.* Precipitation, air temperature, soil moisture and TWSA datasets data have to be extracted for each sub-catchment of the study area. If characterized by different spatial/temporal resolution, these datasets need to be resampled over a common spatial grid/temporal time step prior to be used as input into the model.

To run the STREAM model over the Mississippi river basin, input data have been resampled over the precipitation spatial grid at 0.25° resolution through a bilinear interpolation. Concerning the temporal scale, air temperature, soil moisture and precipitation data are available at daily time step, while monthly TWSA data have been linearly interpolated at daily time step. For each of the 53 Mississippi sub-catchment, the resampled precipitation, soil moisture, air temperature and TWSA data have been extracted (see Figure 1b and 1c).

*3. STREAM model calibration.* In situ river discharge data are used as reference data for the calibration of STREAM model. For Mississippi, the STREAM model has been calibrated at five gauging stations, i.e., the stations 4, 6, 9, 11 and 10. This allowed to identify five sets of STREAM parameters attributed to each catchment according to the river network pathway illustrated in Figure 1a. This means that, for example, to the sub-catchments labelled as 1, 2, 5 to 15, 17, 22, 23, and 30

412 contributing to the gauging station 4 are attributed the parameter set obtained by calibrating the model  
413 against river discharge data observed at station 4; to the sub-catchments 31, 37, 38 and 41 contributing  
414 to gauging station 6 are attributed the parameter set obtained by calibrating the model with respect to  
415 gauging station 6 and so on. Consequently, the sub-catchments highlighted with the same colour in  
416 Figure 1a are assigned the same model parameters, i.e. the parameters that allow to reproduce the  
417 river discharge data observed at the related gage.

418 Once calibrated, the STREAM model has been run to provide continuous daily runoff and river  
419 discharge time series, over each grid pixel and at the outlet section of each sub-catchment,  
420 respectively. By considering the spatial/temporal availability of both in situ and satellite observations,  
421 the entire analysis period covers the maximum common observation period, i.e., from January 2003  
422 to July 2016 at daily time scale. To establish the goodness-of-fit of the model, the modelled river  
423 discharge and runoff timeseries are compared against in situ river discharge and modelled runoff data.

## 424 **5.2 Model Evaluation Criteria and Performance Metrics**

425 The model has been run over a 13.5-year period split into two sub periods: the first 8 years, from  
426 January 2003 to December 2010, are used to calibrate the model. The model is validated, as described  
427 below over the remaining 5.5 years (January 2011 - July 2016).

428 In particular, three different validation schemes have been adopted to assess the robustness of the  
429 STREAM model:

- 430 1. internal validation aimed to test the plausibility of both the model structure and the parameter set  
431 in providing reliable estimates of the hydrological variables against which the model is calibrated.  
432 For this purpose, a comparison between observed and modelled river discharge time series on the  
433 gauging stations used for model calibration has been carried out for both the calibration and  
434 validation sub periods;
- 435 2. cross-validation testing the goodness of the model structure and the calibrated model parameters  
436 to predict hydrological variables at locations not considered in the calibration phase. In this

respect, the cross-validation has been carried out by comparing observed and modelled river discharge time series in gauging stations not considered during the calibration phase;

3. external validation aimed to test the capability of the model “*to get the right answers for the right reasons*” (Kirchner 2006). The rationale behind this concept is that the hydrological models are today highly performing and able to reproduce a lot of hydrological variables. For that, the model performances should not only be evaluated against observed river discharge, but complementary datasets representing internal hydrologic states and fluxes (e.g., soil moisture, evapotranspiration, runoff etc) should be considered. As runoff is a secondary product of the STREAM model, obtained indirectly from the calibration of the river discharge (basin-integrated runoff), the comparison in terms of runoff can be considered as a further external validation of the model. Runoff, differently from river discharge, cannot be directly measured. It is generally modelled through land surface or hydrological models. Its validation requires a comparison against modelled data that, however, suffer from uncertainties (Beck et al., 2017). Based on that, in this study the GRUN runoff dataset described in the paragraph 3.3 has been used for a qualitative comparison.

### 5.3 Performance Metrics

To measure the goodness-of-fit between modelled and observed river discharge data three performance scores have been used:

- the root mean square error relative to the mean, *RRMSE*:

$$RRMSE = \frac{\sqrt{\frac{1}{n} \sum_{j=1}^n (Q_{mod_j} - Q_{obs_j})^2}}{\frac{1}{n} \sum_{j=1}^n (Q_{obs_j})} \quad (8)$$

where  $Q_{obs}$  and  $Q_{mod}$  are the observed and modelled river discharge time series of length  $n$ . *RRMSE* values range from 0 to  $+\infty$ , the lower the *RRMSE*, the better the agreement between observed and modelled data.

- the Pearson correlation coefficient, *rho*, measuring the linear relationship between two variables:

$$rho = \frac{\sum_{j=1}^n (Q_{modj} - \overline{Q_{mod}})(Q_{obsj} - \overline{Q_{obs}})}{\sqrt{\sum_{j=1}^n (Q_{modj} - \overline{Q_{mod}})^2 (Q_{obsj} - \overline{Q_{obs}})^2}} \quad (9)$$

where  $\overline{Q_{obs}}$  and  $\overline{Q_{mod}}$  represent the mean values of  $Q_{obs}$  and  $Q_{mod}$ , respectively. The values of  $rho$  range between  $-1$  and  $1$ ; higher values of  $R$  indicate a better agreement between observed and modelled data.

- the Kling-Gupta efficiency index ( $KGE$ , Gupta et al., 2009), which provides direct assessment of four aspects of river discharge time series, namely shape, timing, water balance and variability.

It is defined as follows:

$$KGE = 1 - \sqrt{(rho - 1)^2 + (\delta - 1)^2 + (\varepsilon - 1)^2} \quad (10)$$

where  $\delta$  is the relative variability and  $\varepsilon$  the bias normalized by the standard deviation between observed and modelled river discharge. The  $KGE$  values range between  $-\infty$  and  $1$ ; the higher the  $KGE$  the better is the agreement between observed and modelled data. Simulations characterized by values of  $KGE$  in the range  $-0.41$  and  $1$  can be assumed as reliable; values of  $KGE$  greater than  $0.5$  have been assumed good with respect to their ability to reproduce observed time series (Thiemig et al., 2013).

#### 5.4 STREAM sensitivity analysis

To investigate how the variation of the STREAM parameters influences the variation of the STREAM model outputs, a global sensitivity analysis has been carried out. Specifically, the Variance-Based sensitivity analysis (VBSA, Sobol 1993) implemented into the Sensitivity Analysis For Everybody toolbox (SAFE, Pianosi et al., 2015, <https://www.safetoolbox.info/>) has been applied. VBSA relies on the variance decomposition and consists of assessing the contributions to the variance of the model output from variations in the parameters. In this study, we use as sensitivity index the first-order (main effect) index, which measures the variance contribution from variations in an individual input factor alone (i.e., excluding interactions with other factors) and the total sensitivity indices, which measure the total contribution of a single input factor or a group of inputs including interactions with all other inputs. The following steps were carried out to execute the VBSA. Firstly, the locality-sensitive

485 hashing (LSH) technique was used to generate 15000 samples from the model parameter space (see  
486 Table 1A). Previous hydrological studies (e.g., [Tang et al., 2007](#)) recommend the LHS sampling  
487 method for its sampling efficiency. Secondly, 15000 STREAM model runs were executed and the  
488 corresponding *KGE* values (11x15000 values, one for each gauging station for each run) were  
489 retained. Thirdly, the parameters and the 15000 *KGE* samples were used in the SAFE toolbox to  
490 compute the sensitivity indices.  
491 For major details on the workflow needed to implement the VBSA the reader is referred to [Noacco](#)  
492 [et al. \(2020\)](#).

## 493 **6. RESULTS**

494 The testing and validation of the STREAM model is presented and discussed in this paragraph  
495 according to the scheme illustrated in paragraph 5.2.

### 496 **6.1 Internal Validation**

497 The performance of the STREAM model over the gauging stations used for calibration is illustrated  
498 in Figure 4 and summarized in Table 2. Figure 4 shows observed and modelled river discharge time  
499 series over the whole study period (2003-2016); in Table 2 the performance scores are evaluated  
500 separately for the calibration and validation sub periods. It is worth noting that the model accurately  
501 predicts the observed river discharge data and is able to give the “right answer” with good modelling  
502 performances. Score values of *KGE* and *rho* over the calibration period are higher than 0.78 for all  
503 the calibrated gauging stations; *RRMSE* is lower than 45% for all the calibrated gauging stations  
504 except for station 9, where it rises up to 66%. The performances remain good even if they are  
505 evaluated over the validation period or the entire study period as indicated by the scores on the top of  
506 each plot of Figure 4.

### 507 **6.2 Cross-validation**

508 The cross-validation has been carried out over the six gauging stations illustrated in Figure 5 not used  
509 in the calibration step. The performance scores on the top of each plot refer to the entire study periods;

the scores split for calibration and validation periods are reported in Table 2. For some river discharge gauging stations the performance is quite low (see, e.g., gauging station 1, 2 and 5) whereas for others the model is able to estimate river discharge data quite accurately (e.g., 7 and 8). In particular, for the gauging stations 1 and 2 even if  $KGE$  reaches values equal to 0.39 and 0.46 for the whole period, respectively, there is not a good agreement between observed and modelled river discharge and the  $\rho$  score is lower than 0.56 for both the stations. The worst performance is obtained over the gauging station 5, with negative  $KGE$  and low  $\rho$  values. These results are certainly influenced by the presence of large dams located upstream to these stations (i.e., Garrison, Gavins Point and Kanopolis dams, see Table 1) which have a strong impact on river discharge: the model, not having a specific module for modelling reservoirs, is not able to accurately reproduce the dynamics of river discharge over regulated river stations. Positive  $KGE$  values are obtained over the gauging stations 3, 7 and 8. In particular, over the gauging station 3 the STREAM model overestimates the observed river discharge due the presence of large dams along the Missouri river, over the Great Plains region. This area is well known from other large-scale hydrological models (e. g., ParFlow-CLM and WRF-Hydro) to be an area with very low performances in terms of river discharge modelling (O'Neill et al., 2020, Tijerina et al., 2021).

Over the gauging station 7, located over the Rock river, a relatively small tributary of the Mississippi river (see Table 1), the STREAM model overestimation has to be attributed to: 1) the different characteristics of the Rock river basin with respect to the entire basin closed to station 6 where the model has been calibrated (see Figure 1a); 2) the small size of the Rock river basin (23'000 km<sup>2</sup>, if compared with GRACE resolution, 160'000 km<sup>2</sup>) for which the model accuracy is expect to be lower. Conversely, the performances over the gauging station 8, whose parameters have been set equal to the ones of gauging station 10, are quite high ( $KGE$  equal to 0.71, 0.81 and 0.78 for the entire, the calibration and the validation period, respectively;  $\rho$  equal to 0.82, 0.84 and 0.83 for the entire, calibration and validation periods, respectively). This outcome demonstrates that under some

535 circumstances, the STREAM model can be used to estimate river discharge in basins not calibrated  
536 over, especially those without upstream dams and with comparable size and land cover.  
537 On overall, the cross-validation results suggest that the performances of STREAM model, as any  
538 hydrological model calibrated against observed data, decrease over the gauging stations not used for  
539 the calibration raising doubts about the robustness of model parameters and whether it is actually  
540 possible to transfer model parameters from one river section to another with different inter-basin  
541 characteristics. A more in-depth investigation about the model calibration procedure, with special  
542 focus on the regionalization of the model parameters, should be carried out but this topic is beyond  
543 the scope of the manuscript.

### 544 **6.3 External Validation**

545 For the external validation, the monthly runoff time series provided by the GRUN datasets have been  
546 compared against the ones computed by the STREAM model. For that, STREAM daily runoff time  
547 series have been aggregated at monthly scale and re-gridded at the same spatial resolution of the  
548 GRUN dataset (0.5°). The comparison is illustrated in Figure 6 for the common period 2003–2014.  
549 Although the two datasets consider different precipitation inputs, the two models agree in identifying  
550 two distinct zones in terms of runoff, i.e., the western dry and the eastern wet area. These two distinct  
551 zones can be clearly identified also in the GSWP3 and TMPA 3B42 V7 precipitation maps (see Figure  
552 S1) used as input in GRUN and STREAM, respectively, stressing that STREAM runoff output is  
553 correctly driven by the input data. However, likely due to the calibration procedure, the STREAM  
554 runoff map appears patchier with respect to GRUN and discontinuities along the sub-basin boundaries  
555 (identified in Figure 1a) can be noted. This should be ascribed to the automatic calibration procedure  
556 of the model that, differently from other calibration techniques (e. g., regionalization procedures),  
557 does not consider the basin physical attributes like soil, vegetation, and geological properties that  
558 govern spatial dynamics of hydrological processes. This calibration procedure can generate sharp  
559 discontinuities even for neighbouring sub-catchments individually calibrated. It leads to

discontinuities in model parameter values and consequently in the modelled hydrological variable (runoff).

#### 6.4 Sensitivity analysis results

The results of the VBSA, are illustrated in Figure 7a in terms of main effect indices and in Figure 7b in terms of total effect. Specifically, the figure refers to Vicksburg station but similar results have been obtained for all the 11 gauging stations in the Mississippi basin. By looking at Figure 7, we observe that the model parameters most influencing the model response are  $\beta$  and  $m$ , i.e., the two parameters controlling the *slow-flow* runoff response of the lower soil storage. In particular, the total effect sensitivity index of these two parameters is higher than the main effect sensitivity index. This means that these two parameters have an effect on the model output not only through their individual variations but also through interactions with other parameters. Instead, the other five parameters ( $\alpha$ ,  $T$ ,  $\gamma$ ,  $C$ ,  $D$  and  $C_m$ ) have low main and total effect indices, and consequently, these parameters have a small effect, both direct and through interactions, on model response. Among these, only the  $\alpha$  parameter shows a slightly high main and total effect sensitivity indices.

This outcome is very important as it allows to clearly distinguish model parameters which values should be carefully determined when calibrating the model ( $\beta$  and  $m$  and partially  $\alpha$ ) from the least sensitive ( $T$ ,  $\gamma$ ,  $C$ ,  $D$  and  $C_m$ ) which values could be set values within the model parameters' range of variability and then excluded during the calibration phase.

### 7. DISCUSSION

In the previous sections, the ability of the STREAM model to estimate river discharge and runoff time series has been presented. In particular, Figures 4, 5 and 6 demonstrate that satellite observations of precipitation, soil moisture and total water storage anomalies can provide accurate daily river discharge estimates for near-natural large basins (absence of upstream dams), and for basins with draining area greater than 160'000 km<sup>2</sup> (see paragraph 6.2), i.e., at spatial/temporal resolution greater



584 than the ones of the TWSA input data (monthly, 160'000 km<sup>2</sup>). This is an important result of the  
585 study as it demonstrates, on one hand, that the model structure is appropriate with respect to the data  
586 used as input and, on the other hand, the great value of information contained into TWSA data that,  
587 even if characterized by limited spatial/temporal resolution, can be used to estimate runoff and river  
588 discharge at basin scale. This finding has been also confirmed by a preliminary sensitivity analysis in  
589 which the STREAM model has been run with different hydrological inputs of precipitation, soil  
590 moisture and total water storage anomaly (not shown here for brevity). In particular, by running the  
591 STREAM model with different input configurations (e.g., by using TMPA 3B42 V7 or CPC data for  
592 precipitation, ESA CCI or Advanced SCATterometer (ASCAT) data for soil moisture, TWSA or ESA  
593 CCI soil moisture data to model the slow-flow river discharge component), we found that STREAM  
594 results are more sensitive to soil moisture data rather than to precipitation input. In addition, by  
595 running STREAM model with soil moisture data as input to model the slow-flow river discharge  
596 component (i.e. without using TWSA data) we found a deterioration of the model results. This  
597 outcome along with the one obtained in the paragraph 6.3, demonstrating the high sensitivity of the  
598 model parameters related to *slow-flow* river discharge component, confirm the paramount role of  
599 TWSA in estimating river discharge. In this respect, the availability of GRACE data up to July 2016  
600 could represent an issue for the model application beyond that date. However, the GRACE-FO along  
601 with the numerous literature studies devoted to fill the GRACE data gap between GRACE and  
602 GRACE-FO (see e.g., [Landerer et al., 2020](#) or [Yi and Sneeuw, 2021](#)), can provide the needed data to  
603 extend the STREAM model application up to present. Further developments in this direction are  
604 expected with the ESA's Next Generation Gravity Mission (NGGM), a candidate Mission of  
605 Opportunity for ESA–NASA cooperation in the frame of the Mass Change and Geosciences  
606 International Constellation (MAGIC) that will enable long-term monitoring of the temporal variations  
607 of Earth's gravity field at relatively high temporal (down to 3 days) and increased spatial resolutions  
608 (up to 100 km). This implies also that time series of GRACE and GRACE-FO can be extended  
609 towards a climate series ([Massotti et al., 2021](#)).

610 By looking at technical reviews of large-scale hydrological models (e.g., Sood and Smakhtin, 2015,  
611 Kauffeldt et al., 2016), it can be noted there are many established models, similar in objective and  
612 limitations to STREAM model, already existing with support and user base (e.g., among others,  
613 Community Land Model, CLM, Oleson et al., 2013; European Hydrological Predictions for the  
614 Environment, E-HYPE, Lindström et al., 2010; H08, Hanasaki et al., 2008, PCR-GLOBWB, van  
615 Beek and Bierkens, 2008; Water – a Global Assessment and Prognosis WaterGAP, Alcamo et al.,  
616 2003; ParFlow-CLM, Maxwell et al., 2015; WRF-Hydro, Gochis et al., 2018; Precipitation-Runoff  
617 Modeling System, PRMS; Markstrom et al., 2015). Some of them, e.g., ParFlow-CLM, WRF-Hydro  
618 or PRMS have been specifically configured across the continental United States and showed good  
619 capability to reproduce observed streamflow data over the Mississippi river basin with performances  
620 decreased throughout the Great Plains (O'Neill et al., 2020, Tijerina et al., 2021) which is consistent  
621 with the results we obtained with the STREAM model. However, with respect to classical  
622 hydrological and land surface models, STREAM is based on a new concept for estimating runoff and  
623 river discharge which relies on the almost exclusive use of satellite observations, and, a simplification  
624 of the processes being modelled.

625 This approach brings several advantages: 1) satellite data implicitly consider the human impact on  
626 the water cycle observing some processes, such as irrigation application or groundwater withdrawals,  
627 that are affected by large uncertainty in classical hydrological models, 2) the satellite technology  
628 grows quickly and hence it is expected that the spatial/temporal resolution and accuracy of satellite  
629 products will be improved in the near future (e.g., 1 km resolution from new satellite soil moisture  
630 products and the next generation gravity mission); the STREAM model is able to fully exploit such  
631 improvements; 3) STREAM model models only the most important processes affecting the  
632 generation of runoff, and considers only the most important variables as input (precipitation, surface  
633 soil moisture and groundwater storage). In other words, the model does not need to parametrize  
634 processes, such as evapotranspiration and percolation and therefore it is an independent modelling

635 approach for simulating runoff and river discharge that can be also exploited for benchmarking and  
636 improving classical land surface and hydrological models.

### 637 **7.1 Strengths and limitations of STREAM model**

638 Hereinafter, the strengths and the main limitations of the STREAM model are discussed.

639 Among the strengths of the STREAM model it is worth highlighting:

640 **Simplicity.** The STREAM model structure: 1) limits the input data required. Only precipitation, air  
641 temperature, soil moisture and TWSA data are needed as input whereas LSM/GHMs require many  
642 additional inputs such as wind speed, shortwave and longwave radiation, pressure and relative  
643 humidity; 2) limits and simplifies the processes to be modelled for runoff and river discharge  
644 simulation. Processes like evapotranspiration or percolation, are not modelled therefore avoiding the  
645 need of using sophisticated and highly parameterized equations (e.g., Penman-Monteith for  
646 evapotranspiration, [Allen et al.,1998](#)); 3) limits the number of parameters (only 8 parameters have to  
647 be calibrated) thus simplifying the calibration procedure and potentially reduces the model  
648 uncertainties related to the estimation of parameter values.

649 In particular, the STREAM model is even simpler than the classical semi-distributed conceptual  
650 hydrological models available in literature. As an example, for the comparison we could refer to the  
651 Hydrologiska Byråns Vattenbalansavdelning model (HBV, Bergström 1995) or to the Hydrologic  
652 Engineering Center – Hydrologic Modeling System (HEC-HMS, [Feldman, 2000](#)). HBV model counts  
653 14 parameters to be calibrated and needs precipitation, air temperature and potential  
654 evapotranspiration as input data. Similar input data are required for HEC-HMS which counts 23  
655 parameters. Both the models, uses conceptual equations to estimate the soil losses and to model the  
656 soil water storage.

657 **Versatility.** The STREAM model is a versatile model suitable for daily runoff and river discharge  
658 estimation over sub-basins characterized by different physiographic/climatic characteristics (see e.g.,  
659 the outcomes obtained for the gages 9 and 11 located in the driest and wetter part of the Mississippi  
660 basin). This aspect is paramount as it gives an insight about the potential of the model to be extended

661 at the global scale. Moreover, the model can be easily adapted to ingest input data with  
662 spatial/temporal resolution different from the one tested in this study (0.25°/daily). For instance,  
663 satellite missions with higher space/time resolution (e.g., GPM Final Run, ASCAT and NGGM-  
664 MAGIC) or near-real time products (e.g., GPM Early Run, EUMETSAT H16, GRACE European  
665 Gravity Service for Improved Emergency Management, EGSIM GRACE data Jäggi et al., 2019)  
666 could be considered.

667 Additionally, the STREAM model shows highly flexibility as: 1) it can accommodate application  
668 domains comprising single or multiple basins of any size; and 2) the sub-catchment delineation  
669 procedure can be easily adapted to introduce intermediate outlets along the river in correspondence  
670 of gages with available observed river discharge data, useful for model calibration.

671 **Low computational cost.** Due to its simplicity and the limited number of parameters to be calibrated,  
672 the computational effort for the STREAM model is very limited (model runs requiring seconds to  
673 minutes). For instance, a run of the STREAM model over the presented case study takes less than 2  
674 seconds on a machine with 16 GB RAM and 4 Core.

675 However, some limitations have to be acknowledged for the current version of the STREAM model:

676 **Presence of reservoir, diversion, dams or flood plain.** As the STREAM model does not explicitly  
677 consider the presence of discontinuity elements along the river network (e. g, reservoir, dam or  
678 floodplain), river discharge estimates obtained for gauging stations located downstream of such  
679 elements might be inaccurate (see, e.g., gauging stations 1 and 2 in Figure 5).

680 **Snow modelling.** A potential limitation of the current version of the STREAM model is related to  
681 the rain/snow differentiation, based on the degree-day coefficient. A different scheme based e.g., on  
682 the wet bulb temperature like in IMERG (Wang et al., 2019; Arabzadeh and Behrangi, 2021), could  
683 be investigated in future developments.

684 **Need of in situ data for model calibration and robustness of model parameters.** As discussed in  
685 the results paragraph, the parameter values of the STREAM model are set through an automatic  
686 calibration procedure aimed at minimizing the differences between modelled and observed river

687 discharge. The main drawbacks of this parameterization technique are a poor predictability of state  
688 variables and fluxes at locations and periods not considered in the calibration, and the presence of  
689 sharp discontinuities along sub-basin boundaries in state flux and parameter fields (e.g., Merz and  
690 Blöschl, 2004). To overcome these issues, several regionalization procedures, as for instance  
691 summarized in Cislaghi et al. (2020), could be conveniently applied to transfer model parameters  
692 from hydrologically similar catchments to a catchment of interest. In particular, the regionalization  
693 of model parameters could allow to, firstly, estimate river discharge and runoff time series over  
694 ungauged basins overcoming the need of river discharge data recorded from in-situ networks,  
695 secondly, estimate the model parameter values through a physically consistent approach, linking them  
696 to the characteristics of the basins and, thirdly, solve the problem of discontinuities in the model  
697 parameters, avoiding to obtain patchy unrealistic runoff maps. As this aspect requires additional  
698 investigations and it is beyond the paper purpose, it will not be tackled here.

## 699 **8. CONCLUSIONS**

700 This study presents a new conceptual hydrological model, STREAM, for runoff and river discharge  
701 estimation. By using as input satellite data of precipitation, soil moisture and total water storage  
702 anomalies, the model has been able to provide accurate daily river discharge and runoff estimates at  
703 the outlet river section and the inner river sections and over a  $0.25^{\circ} \times 0.25^{\circ}$  spatial grid of the  
704 Mississippi river basin. In particular, the model is suitable to reproduce:

- 705 1. river discharge time series over the calibrated river section with good performances both in  
706 calibration and validation periods;
- 707 2. river discharge time series over river sections not used for calibration and not located downstream  
708 dams or reservoirs;
- 709 3. runoff time series with a quite good agreement with respect to the well-established GRUN  
710 observational-based dataset used for comparison.

711 The integration of observations of soil moisture, precipitation and total water storage anomalies is a  
712 first alternative method for river discharge and runoff estimation with respect to classical methods  
713 based on the use of TWSA-only (suitable for river basins larger than 160'000 km<sup>2</sup>, monthly time  
714 scale) or on classical LSMs (Cai et al., 2014).

715 Moreover, although simple, the model has demonstrated a great potential to be easily applied over  
716 sub-basins with different climatic and topographic characteristics, suggesting also the possibility to  
717 extend its application to other basins. In particular, the analysis over basins with high human impact,  
718 where the knowledge of the hydrological cycle and the river discharge monitoring is very important,  
719 deserves special attention. Indeed, as the STREAM model is directly ingesting observations of soil  
720 moisture and total water storage data, it allows the modeller to neglect processes that are implicitly  
721 accounted for in the input data. Therefore, human-driven processes (e.g., irrigation, land use change),  
722 that are typically very difficult to model due to missing information and might have a large impact  
723 on the hydrological cycle, hence on runoff, could be implicitly modelled. The application of the  
724 STREAM model on a larger number of basins with different climatic- physiographic characteristics  
725 (e.g., including more arid basins, snow-dominated, lots of topography, heavily managed) along with  
726 the results about the sensitivity analysis of the model parameters, will allow to investigate the  
727 possibility to regionalize the model parameters and overcome the limitations of the automatic  
728 calibration procedure highlighted in the discussion paragraph.

## 729 **AUTHOR CONTRIBUTION**

730 S.C. performed the analysis and wrote the manuscript. G.G. collected the data and helped in  
731 performing the analysis; C.M, L.B., A.T., N.S., H.H.F., C.M., M.R. and J.B. contributed to the  
732 supervision of the work. All authors discussed the results and contributed to the final manuscript.

733 **CODE AVAILABILITY**

734 The STREAM model version 1.3, with a short user manual, is freely downloadable in Zenodo  
735 (<https://zenodo.org/record/4744984>, doi: 10.5281/zenodo.4744984). The STREAM model code is  
736 distributed through M language files, but it could be run with different interpreters of M language,  
737 like the GNU Octave (freely downloadable here <https://www.gnu.org/software/octave/download>).

738 **DATA AVAILABILITY**

739 All data and codes used in the study are freely available online. Air temperature data are available at  
740 <https://psl.noaa.gov/data/gridded/data.cpc.globaltemp.html> (last access 25/11/202). In situ river  
741 discharge data have been taken from the Global Runoff Data Center (GRDC,  
742 [https://www.bafg.de/GRDC/EN/Home/homepage\\_node.html](https://www.bafg.de/GRDC/EN/Home/homepage_node.html) (last access 25/11/202). Precipitation  
743 and soil moisture data are available from <http://pmm.nasa.gov/data-access/downloads/trmm> and  
744 <https://esa-soilmoisture-cci.org/>, respectively.

745 **COMPETING INTERESTS**

746 The authors declare that they have no conflict of interest.

747 **ACKNOWLEDGMENTS**

748 The authors wish to thank the Global Runoff Data Centre (GRDC) for providing most of the  
749 streamflow data throughout Europe. The authors gratefully acknowledge support from ESA through  
750 the STREAM Project (EO Science for Society element Permanent Open Call contract n°  
751 4000126745/19/I-NB).

752

## 753 REFERENCE

- 754 Albergel, C., Rüdiger, C., Carrer, D., Calvet, J. C., Fritz, N., Naeimi, V., Batalis, Z., and Hasenauer, S.: An evaluation  
755 of ASCAT surface soil moisture products with in-situ observations in southwestern France, *Hydrol. Earth Syst. Sci.*,  
756 13, 115–124, <https://doi.org/doi:10.5194/hess-13-115-2009>, 2009.
- 757 Alcamo, J., Döll, P., Henrichs, T., Kaspar, F., Lehner, B., Rösch, T., & Siebert, S.: Development and testing of the  
758 WaterGAP 2 global model of water use and availability, *Hydrol. Sci. J.*, 48(3), 317–337,  
759 <https://doi.org/10.1623/hysj.48.3.317.45290>, 2003.
- 760 Alexander, J. S., Wilson, R. C., and Green, W. R.: A brief history and summary of the effects of river engineering and  
761 dams on the Mississippi River system and delta (p. 53), US Department of the Interior, US Geological Survey,  
762 <https://doi.org/10.3133/cir1375>, 2012.
- 763 Allen, R.G., Pereira, L. S., Raes, D., and Smith, M.: Crop evapotranspiration — guidelines for computing crop water  
764 requirements. FAO Irrigation & Drainage Paper 56. FAO, Rome, 1988.
- 765 Arabzadeh, A., and Behrangi, A.: Investigating Various Products of IMERG for Precipitation Retrieval Over Surfaces  
766 With and Without Snow and Ice Cover, *Remote Sens.*, 13(14), 2726; <https://doi.org/10.3390/rs13142726>, 2021.
- 767 Balsamo, G., A. Beljaars, K. Scipal, P. Viterbo, B. vanden Hurk, M. Hirschi, and A. K. Betts: A revised hydrology for  
768 the ECMWF model: Verification from field site to terrestrial water storage and impact in the integrated forecast  
769 system, *J. Hydrometeorol.*, 10(3), 623–643, <https://doi.org/doi:10.1175/2008JHM1068.1>, 2009.
- 770 Barbarossa, V., Huijbregts, M. A., Beusen, A. H., Beck, H. E., King, H., and Schipper, A. M.: FLO1K, global maps of  
771 mean, maximum and minimum annual streamflow at 1 km resolution from 1960 through 2015, *Scientific Sci. Data*,  
772 55, 180052, <https://doi.org/10.1038/sdata.2018.52>, 2018.
- 773 Beck, H. E., van Dijk, A. I., de Roo, A., Dutra, E., Fink, G., Orth, R., and Schellekens, J.: Global evaluation of runoff  
774 from ten state-of-the-art hydrological models, *Hydrol. Earth Syst. Sci.*, 21(6), 2881–2903. <https://doi.org/doi:10.5194/hess-21-2881-2017>, 2017.
- 775
- 776 Berghuijs, W. R., Woods, R. A., Hutton, C. J., and Sivapalan, M.: Dominant flood generating mechanisms across the  
777 United States, *Geophys. Res. Lett.*, 43, 4382–4390, <https://doi.org/10.1002/2016GL068070>, 2016.
- 778 Berghuijs, W. R., Woods, R. A., Hutton, C. J., and Sivapalan, M.: Dominant flood generating mechanisms across the  
779 United States, *Geophys. Res. Lett.*, 43, 4382–4390, <https://doi.org/10.1002/2016GL068070>, 2016.
- 780 Bergström, S (1995) The HBV model. In Singh, VP ed. Computer models of watershed hydrology. Water Resources  
781 Publications, Highlands Ranch, CO, 443–476
- 782 Berthet, L., Andréassian, V., Perrin, C., and Javelle, P.: How crucial is it to account for the antecedent moisture conditions  
783 in flood forecasting? Comparison of event-based and continuous approaches on 178 catchments, *Hydrol. Earth Syst.*  
784 *Sci.*, 13(6), 819–831, 2009.
- 785 Blöschl, G., Sivapalan, M., Wagener, T., Viglione, A., and Savenije, H. H. G. (Eds.): Runoff predictions in ungauged  
786 basins: A synthesis across processes, places and scales, Cambridge: Cambridge University Press, 2013.
- 787 Bober, W. Introduction to Numerical and Analytical Methods with MATLAB for Engineers and Scientists; CRC Press,  
788 Inc.: Boca Raton, FL, USA, <https://doi.org/10.1201/b16030>, 2013.
- 789 Botter, G., Peratoner, F., Porporato, A., Rodriguez-Iturbe, I., and Rinaldo, A.: Signatures of large-scale soil moisture  
790 dynamics on streamflow statistics across U.S. Climate regimes, *Water Resour. Res.*, 43, W11413,  
791 <https://doi.org/doi:10.1029/2007WR006162>, 2007b.
- 792 Botter, G., Porporato, A., Daly, E., Rodriguez-Iturbe, I., and Rinaldo, A.: Probabilistic characterization of base flows in  
793 river basins: Roles of soil, vegetation, and geomorphology, *Water Resour. Res.*, 43, W06404,  
794 <https://doi.org/doi:10.1029/2006WR005397>, 2007a.
- 795 Brocca, L., Ciabatta, L., Massari, C., Camici, S., and Tarpanelli, A.: Soil moisture for hydrological applications: open  
796 questions and new opportunities, *Water*, 9(2), 140, <https://doi.org/10.3390/w9020140>, 2017.



797 Brocca, L., Melone, F., and Moramarco, T.: Distributed rainfall-runoff modelling for flood frequency estimation and  
798 flood forecasting, *Hydrol. Process.*, 25(18), 2801-2813, <https://doi.org/10.1002/hyp.8042>, 2011.

799 Brocca, L., Melone, F., and Moramarco, T.: On the estimation of antecedent wetness conditions in rainfall-runoff  
800 modelling, *Hydrol. Process.*, 22 (5), 629-642, doi:10.1002/hyp.6629. <https://doi.org/10.1002/hyp.6629>, 2008.

801 Brocca, L., Melone, F., Moramarco, T., and Morbidelli, R.: Antecedent wetness conditions based on ERS scatterometer  
802 data, *J. Hydrol.*, 364(1-2), 73-87, <https://doi.org/10.1016/j.jhydrol.2008.10.007>, 2009.

803 Cai, X., Yang, Z. L., David, C. H., Niu, G. Y., and Rodell, M.: Hydrological evaluation of the Noah-MP land surface  
804 model for the Mississippi River Basin, *J. Geophys. Res. Atmos.*, 119(1), 23-38,  
805 <https://doi.org/10.1002/2013JD020792>, 2014.

806 Cislighi, A., Masseroni, D., Massari, C., Camici, S., and Brocca, L.: Combining a rainfall-runoff model and a  
807 regionalization approach for flood and water resource assessment in the western Po Valley, Italy, *Hydrol. Sci. J.*,  
808 65(3), 348-370, <https://doi.org/10.1080/02626667.2019.1690656>, 2020.

809 Corradini C, Morbidelli R, Saltalippi C, Melone F. 2002. An adaptive model for flood forecasting on medium size basins.  
810 In *Applied Simulation and Modelling*, Ubertini L (ed). IASTED Acta Press: Anaheim (CA); 555-559.

811 Crochemore, L., Isberg, K., Pimentel, R., Pineda, L., Hasan, A., and Arheimer, B.: Lessons learnt from checking the  
812 quality of openly accessible river flow data worldwide, *Hydrol. Sci. J.*, 65(5), 699-711,  
813 <https://doi.org/10.1080/02626667.2019.1659509>, 2020.

814 Crow, W. T., Bindlish, R., and Jackson, T. J.: The added value of spaceborne passive microwave soil moisture retrievals  
815 for forecasting rainfall-runoff partitioning, *Geophys. Res. Lett.*, 32(18), <https://doi.org/10.1029/2005GL023543>,  
816 2005.

817 Döll, P., F.Kaspar, and B.Lehner: A global hydrological model for deriving water availability indicators: Model tuning  
818 and validation, *J. Hydrol.*, 270(1-2), 105-134, [https://doi.org/doi:10.1016/S0022-1694\(02\)00283-4](https://doi.org/doi:10.1016/S0022-1694(02)00283-4), 2003.

819 Dorigo, W., Wagner, W., Albergel, C., Albrecht, F., Balsamo, G., Brocca, L., Chung, D., Ertl, M., Forkel, M., Gruber, A.,  
820 Haas, D., Hamer, P., Hirschi, M., Ikonen, J., de Jeu, R., Kidd, R., Lahoz, W., Liu, Y.Y., Miralles, D., Mistelbauer, T.,  
821 Nicolai-Shaw, N., Parinussa, R., Pratola, C., Reimer, C., van der Schalie, R., Seneviratne, S.I., Smolander, T., and  
822 Lecomte, P.: ESA CCI Soil Moisture for improved Earth system understanding: state-of-the art and future directions.,  
823 *Remote Sens. Environ.*, 203, 185-215, <https://doi.org/10.1016/j.rse.2017.07.001>, 2017.

824 Dyer, J.: Snow depth and streamflow relationships in large North American watersheds, *J. Geophys. Res.*, 113, D18113,  
825 <https://doi.org/10.1029/2008JD010031>, 2008.

826 Entekhabi, D., Njoku, E. G., O'Neill, P. E., Kellogg, K. H., Crow, W. T., Edelstein, W. N., ... and Van Zyl, J.: The soil  
827 moisture active passive (SMAP) mission. *Proceedings of the Institute of Electrical and Electronics Engineers (IEEE)*,  
828 98(5), 704-716. <https://doi.org/doi:10.1109/JPROC.2010.2043918>, 2010.

829 Famiglietti, J. S., and Rodell, M.: Water in the balance, *Science*, 340(6138), 1300-1301,  
830 <https://doi.org/10.1126/science.1236460>, 2013.

831 Famiglietti, J.S., and Wood, E. F.: Multiscale modeling of spatially variable water and energy balance processes, *Water*  
832 *Resour. Res.*, 30, 3061-3078, <https://doi.org/10.1029/94WR01498>, 1994.

833 Fan, Y. and Van den Dool, H. A: Global monthly land surface air temperature analysis for 1948-present, *J. Geophys.*  
834 *Res. Atmos.*, 113, D01103, <https://doi.org/10.1029/2007JD008470>, 2008.

835 Fekete, B. M., Looser, U., Pietroniro, A., and Robarts, R. D.: Rationale for monitoring discharge on the ground, *J.*  
836 *Hydrometeorol.*, 13, 1977-1986, <https://doi.org/10.1175/JHM-D-11-0126.1>, 2012.

837 Feldman, A. D. (2000). *Hydrologic modeling system HEC-HMS: technical reference manual*. US Army Corps of  
838 Engineers, Hydrologic Engineering Center.

839 Georgakakos KP, and Baumer OW.: Measurement and utilization of onsite soil moisture data, *J. Hydrol.*, 184: , 131-152,  
840 [https://doi.org/10.1016/0022-1694\(95\)02971-0](https://doi.org/10.1016/0022-1694(95)02971-0), 1996.

841 Ghiggi, G., Humphrey, V., Seneviratne, S. I., and Gudmundsson, L.: GRUN: an observation-based global gridded runoff  
842 dataset from 1902 to 2014, *Earth Syst. Sci. Data*, 11, 1655-1674 *Earth System Science Data*, 11(4), 1655-1674,  
843 <https://doi.org/10.5194/essd-11-1655-2019>, 2019.

844 Ghotbi, S., Wang, D., Singh, A., Blöschl, G., and Sivapalan, M.: A New Framework for Exploring Process Controls of  
845 Flow Duration Curves, *Water Resour. Res.* *Water Resources Research*, 56(1), <https://doi.org/e2019WR026083>, 2020.

846 Gochis, D. J., Barlage, M., Dugger, A., FitzGerald, K., Karsten, L., McAllister, M., et al. (2018). The WRF-Hydro  
847 modeling system technical description, (Version 5.0). NCAR Technical Note. Retrieved from  
848 <https://ral.ucar.edu/sites/default/files/public/WRFHydroV5TechnicalDescription.pdf>

849 Gudmundsson, L., and Seneviratne, S. I.: Observation-based gridded runoff estimates for Europe (E-RUN version 1.1),  
850 *Earth Syst. Sci. Data*, 8, 279–295, <https://doi.org/10.5194/essd-8-279-2016>, 8(2), 279-2952016, 2016.

851 Gudmundsson, L., Tallaksen, L. M., Stahl, K., Clark, D. B., Du-mont, E., Hagemann, S., Bertrand, N., Gerten, D., Heinke,  
852 J., Hanasaki, N., Voss, F., and Koirala, S.: Comparing Large-Scale Hydrological Model Simulations to Observed  
853 Runoff Percentiles in Europe, *J. Hydrometeorol.*, 13, 604–62, <https://doi.org/10.1175/JHM-D-11-083.1>, 2012b.

854 Gudmundsson, L., Wagener, T., Tallaksen, L. M., and Engeland, K.: Evaluation of nine large-scale hydrological models  
855 with respect to the seasonal runoff climatology in Europe, *Water Resour. Res.*, 48(11),  
856 <https://doi.org/10.1029/2011WR010911>, 2012a.

857 Gupta VK, Waymire E, and Wang CT.: A representation of an instantaneous unit hydrograph from geomorphology, *Water*  
858 *Resour. Res.*, 16: 855–862, <https://doi.org/doi:10.1029/WR016i005p00855>, 1980.

859 Gupta, H. V., Kling, H., Yilmaz, K. K., and Martinez, G. F.: Decomposition of the mean squared error and NSE  
860 performance criteria: Implications for improving hydrological modelling, *J. Hydrol.*, 377(1-2), 80-91,  
861 <https://doi.org/10.1016/j.jhydrol.2009.08.003>, 2009.

862 Haddeland, I., Heinke, J., Voß, F., Eisner, S., Chen, C., Hagemann, S., and Ludwig, F.: Effects of climate model radiation,  
863 humidity and wind estimates on hydrological simulations, *Hydrol. Earth Syst. Sci.*, 16(2), 305-318,  
864 <https://doi.org/10.5194/hess-16-305-2012>, 2012.

865 Hanasaki, N., Kanae, S., Oki, T., Masuda, K., Motoya, K., Shirakawa, N., ... , and Tanaka, K. :An integrated model for  
866 the assessment of global water resources–Part 1: Model description and input meteorological forcing, *Hydrol. Earth*  
867 *Syst. Sci.*, 12(4), 1007-1025, <https://doi.org/10.5194/hess-12-1007-2008>, 2008.

868 Hastie, T., Tibshirani, R., and Friedman, J. H.: *The Elements of Statistical Learning – Data Mining, Inference, and*  
869 *Prediction*, Second Edition, Springer Series in Statistics, Springer, New York, 2nd Edn., available at: [http://www-](http://www-stat.stanford.edu/~tibs/ElemStatLearn/)  
870 [stat.stanford.edu/~tibs/ElemStatLearn/](http://www-stat.stanford.edu/~tibs/ElemStatLearn/) (last access: 5 July 2016)., 2009.

871 Hong, Y., Adler, R. F., Hossain, F., Curtis, S., and Huffman, G. J.: A first approach to global runoff simulation using  
872 satellite rainfall estimation, *Water Resour. Res.*, 43(8), <https://doi.org/10.1029/2006WR005739>, 2007.

873 Horton, R. E.: Hydrological approach to quantitative morphology, *Geol. Soc. Am. Bull.*, 56, 275-370, 1945.

874 Houborg, R., Rodell, M., Li, B., Reichle, R., and Zaitchik, B. F.: Drought indicators based on model-assimilated Gravity  
875 Recovery and Climate Experiment (GRACE) terrestrial water storage observations, *Water Resour. Res.*, 48(7),  
876 <https://doi.org/10.1029/2011WR011291>, 2012.

877 Hu GR., and Li XY.: Subsurface Flow. In: Li X., Vereecken H. (eds) *Observation and Measurement. Ecohydrology.*  
878 Springer, Berlin, Heidelberg. [https://doi.org/10.1007/978-3-662-47871-4\\_9-1](https://doi.org/10.1007/978-3-662-47871-4_9-1), 2018.

879 Huffman, G. J., Adler, R. F., Bolvin, D. T., Gu, G. J., Nelkin, E. J., Bowman, K. P., Hong, Y., Stocker, E. F. and Wolff,  
880 D. B.: The TRMM Multisatellite Precipitation Analysis (TMPA): Quasi-Global, Multiyear, Combined-Sensor  
881 Precipitation Estimates at Fine Scales, *J. Hydrometeorol.*, 8 (1): 38–55. <https://doi.org/doi:10.1175/jhm560.1>, 2007.

882 Huffman, G. J., Bolvin, D. T., Braithwaite D., Hsu K., Joyce R. , Kidd C., Nelkin Eric J., Sorooshian S., Tan J., and Xie  
883 P.: NASA Global Precipitation Measurement (GPM) Integrated Multi-satellitE Retrievals for GPM (IMERG),.  
884 [https://docserver.gesdisc.eosdis.nasa.gov/public/project/GPM/IMERG\\_ATBD\\_V06.pdf](https://docserver.gesdisc.eosdis.nasa.gov/public/project/GPM/IMERG_ATBD_V06.pdf), 2019.

885 Huffman, G. J., Stocker, E. F., Bolvin, D. T., Nelkin, E. J., and Adler, R. F.: TRMM Version 7 3B42 and 3B43 Data Sets.  
886 NASA/GSFC, Greenbelt, MD, 2014.

887 Jäggi, A., Weigelt, M., Flechtner, F., Güntner, A., Mayer-Gürr, T., Martinis, S., ... and Shabanloui, A.: European gravity  
888 service for improved emergency management (EGSIEM)—from concept to implementation. *Geophysical journal*  
889 *international*, 218(3), 1572-1590, 2019, <https://doi.org/10.1093/gji/ggz238>.

890 Kauffeldt, A., Wetterhall, F., Pappenberger, F., Salamon, P., & Thielen, J.: Technical review of large-scale hydrological  
891 models for implementation in operational flood forecasting schemes on continental level, *Environ. Model. Softw.*, 75,  
892 68-76, <https://doi.org/10.1016/j.envsoft.2015.09.009>, 2016.

893 Kim, H., Watanabe, S., Chang, E. C., Yoshimura, K., Hirabayashi, J., Famiglietti, J., and Oki, T.: Global Soil Wetness  
894 Project Phase 3 Atmospheric Boundary Conditions (Experiment 1) [Data set], Data Integration and Analysis System  
895 (DIAS), <https://doi.org/10.20783/DIAS.501>, 2017.

896 Kirchner, J. W.: Getting the right answers for the right reasons: Linking measurements, analyses, and models to advance  
897 the science of hydrology, *Water Resour. Res.*, 42(3), <https://doi.org/10.1029/2005WR004362>, 2006.

898 Klees, R., Revtova, E. A., Gunter, B.C. , Ditmar, P., Oudman, E., Winsemius H. C., and Savenije H.H.G.: The design of  
899 an optimal filter for monthly GRACE gravity models, *Geoph. J. Intern.*, 175 (2): 417–432,  
900 <https://doi.org/10.1111/j.1365-246X.2008.03922.x>, 2008

901 Kling, H., Fuchs, M., and Paulin, M.: Runoff conditions in the upper Danube basin under an ensemble of climate change  
902 scenarios, *J. Hydrol.*, 424, 264-277, <https://doi.org/doi:10.1016/j.jhydrol.2012.01.011>, 2012.

903 Landerer, F. W., and Swenson, S. C.: Accuracy of scaled GRACE terrestrial water storage estimates, *Water Resour. Res.*,  
904 48(4), <https://doi.org/10.1029/2011WR011453>, 2012.

905 Lehner, B., C. Reidy Liermann, C. Revenga, C. Vörösmarty, B. Fekete, P. Crouzet, P. Döll, M. Endejan, K. Frenken, J.  
906 Magome, C. Nilsson, J.C. Robertson, R. Rodel, N. Sindorf, and D. Wisser.: High-resolution mapping of the world's  
907 reservoirs and dams for sustainable river-flow management, *Front. Ecol. Environ.*, 9 (9): 494-502,  
908 <https://doi.org/10.1890/100125>, 2011.

909 Lindström, G., Pers, C., Rosberg, J., Strömqvist, J., & Arheimer, B.: Development and testing of the HYPE (Hydrological  
910 Predictions for the Environment) water quality model for different spatial scales, *Hydrol. Res.*, 41(3-4), 295-319,  
911 <https://doi.org/10.2166/nh.2010.007>, 2010.

912 Long, D., Longuevergne, L., and Scanlon, B. R.: Uncertainty in evapotranspiration from land surface modeling, remote  
913 sensing, and GRACE satellites, *Water Resour. Res.*, 50(2), 1131-1151, <https://doi.org/10.1002/2013WR014581>,  
914 2014.

915 Lorenz, C., H. Kunstmann, H., B. Devaraju, B., Tourian, M. J., N. Sneeuw, N., and J. Riegger, J.: Large-Scale Runoff  
916 from Landmasses: A Global Assessment of the Closure of the Hydrological and Atmospheric Water Balances., *J.*  
917 *Hydrometeor.*, 15, 2111–2139, <https://doi.org/doi:10.1175/JHM-D-13-0157.1>, 2014.

918 Luthcke, S.B., Sabaka, T.J., Loomis, B.D., Arendt, A.A., McCarthy, J.J., and Camp, J.: Antarctica, Greenland and Gulf  
919 of Alaska land-ice evolution from an iterated GRACE global mascon solution, *J. Glaciol.*, Vol. 59, No. 216, 613-631,  
920 2013 <https://doi.org/doi:10.3189/2013JoG12J147>, 2013.

921 Markstrom, S.L., Regan, R.S., Hay, L.E., Viger, R.J., Webb, R.M.T., Payn, R.A., and LaFontaine, J.H.: PRMS-IV, the  
922 precipitation-runoff modeling system, version 4: U.S. Geological Survey Techniques and Methods, book 6, chap. B7,  
923 158 p., <https://doi.org/10.3133/tm6B7>, 2015

924 Massari, C., Brocca, L., Barbetta, S., Papathanasiou, C., Mimikou, M., and Moramarco, T.: Using globally available soil  
925 moisture indicators for flood modelling in Mediterranean catchments, *Hydrol. Earth Syst. Sci.*, 18(2), 839,  
926 <https://doi.org/10.5194/hess-18-839-2014>, 2014.

927 Massari, C., Brocca, L., Barbetta, S., Papathanasiou, C., Mimikou, M., and Moramarco, T.: Using globally available soil  
928 moisture indicators for flood modelling in Mediterranean catchments, *Hydrol. Earth Syst. Sci.*, 18(2), 839,  
929 <https://doi.org/10.5194/hess-18-839-2014>, 2014.

930 Massari, C., Brocca, L., Tarpanelli, A., Hong, Y., Crow, W., Ciabatta, L., Camici, S., Barbetta, S., and Moramarco, T.:  
931 Global surface runoff estimation in near real time by using SMAP and GPM, poster at SMAP conference, 2016.

932 Massari, C., Brocca, L., Tarpanelli, A., Hong, Y., Crow, W., Ciabatta, L., Camici, S., Barbetta, S., and Moramarco, T.:  
933 Global surface runoff estimation in near real time by using SMAP and GPM, poster at SMAP conference, 2016.

934 Massotti, L., Siemes, C., March, G., Haagmans, R., and Silvestrin, P.: Next generation gravity mission elements of the  
935 mass change and geoscience international constellation: From orbit selection to instrument and mission  
936 design. *Remote Sensing*, 13(19), 3935. <https://doi.org/10.3390/rs13193935>, 2021.

937 Maxwell, R. M., Condon, L. E., and Kollet, S. J.: A high-resolution simulation of groundwater and surface water over  
 938 most of the continental US with the integrated hydrologic model ParFlow v3, *Geosci. Model Dev.*, 8, 923–937,  
 939 <https://doi.org/10.5194/gmd-8-923-2015>, 2015.

940 Maxwell, R. M., Condon, L. E., and Kollet, S. J.: A high-resolution simulation of groundwater and surface water over  
 941 most of the continental US with the integrated hydrologic model ParFlow v3, *Geosci. Model Dev.*, 8, 923–937,  
 942 <https://doi.org/10.5194/gmd-8-923-2015>, 2015.

943 Merz, R., and Blöschl, G.: A regional analysis of event runoff coefficients with respect to climate and catchment  
 944 characteristics in Austria, *Water Resour. Res.*, 45(1), <https://doi.org/10.1029/2008WR007163>, 2009.

945 Mueller Schmied, H., Adam, L., Eisner, S., Fink, G., Flörke, M., Kim, H., ... and Song, Q.: Variations of global and  
 946 continental water balance components as impacted by climate forcing uncertainty and human water use, *Hydrol. Earth  
 947 Syst. Sci.*, 20(7), 2877–2898, <https://doi.org/10.5194/hess-20-2877-2016>, 2016.

948 Muneeppeerakul, R., Azale, S., Botter, G., Rinaldo, A., and Rodriguez-Iturbe, I.: Daily streamflow analysis based on a  
 949 two-scaled gamma pulse model, *Water Resour. Res.*, 46(11), <https://doi.org/10.1029/2010WR009286>, 2010.

950 Nash, J. E.: The form of the instantaneous unit hydrograph, IASH publication no. 45, 3–4, 114–121, 1957.

951 Natural Resources Conservation Service (NRCS): Urban hydrology for small watersheds, Tech. Release 55, 2nd ed., U.S.  
 952 Dep. of Agric., Washington, D. C. (available at [ftp://ftp.wcc.nrcs.usda.gov/downloads/](ftp://ftp.wcc.nrcs.usda.gov/downloads/hydrology_hydraulics/tr55/tr55.pdf)  
 953 [hydrology\\_hydraulics/tr55/tr55.pdf](ftp://ftp.wcc.nrcs.usda.gov/downloads/hydrology_hydraulics/tr55/tr55.pdf)), 1986.

954 Noacco, V., Sarrazin, F., Pianosi, F., & Wagener, T.: Matlab/R workflows to assess critical choices in Global Sensitivity  
 955 Analysis using the SAFE toolbox. *MethodsX*, 6, 2258–2280, 2019, <https://doi.org/10.1016/j.mex.2019.09.033>.

956 Oleson, K., Lawrence, D. M., Bonan, G. B., Drewniak, B., Huang, M., Koven, C. D., ... Yang, Z. -L.: Technical  
 957 description of version 4.5 of the Community Land Model (CLM) (No. NCAR/TN-503+STR).  
 958 <http://dx.doi.org/10.5065/D6RR1W7M>, 2013.

959 Orth, R., and Seneviratne, S. I.: Introduction of a simple-model-based land surface dataset for Europe, *Environ. Res. Lett.*,  
 960 10(4), 044012, <https://doi.org/10.1088/1748-9326/10/4/044012>, 2015.

961 Pellet, V., Aires, F., Munier, S., Fernández Prieto, D., Jordá, G., Dorigo, W. A., ... and Brocca, L.: Integrating multiple  
 962 satellite observations into a coherent dataset to monitor the full water cycle—application to the Mediterranean region.,  
 963 *Hydrol. Earth Syst. Sci.*, 23(1), 465–491, <https://doi.org/10.5194/hess-23-465-2019>, 2019.

964 Pianosi, F., Sarrazin, F., Wagener, T. (2015), A Matlab toolbox for Global Sensitivity Analysis, *Environmental Modelling  
 965 & Software*, 70, 80–85, <https://doi.org/10.1016/j.envsoft.2015.04.009>.

966 Prudhomme, C., Giuntoli, I., Robinson, E. L., Clark, D. B., Arnell, N. W., Dankers, R., ... and Hagemann, S.: Hydrological  
 967 droughts in the 21st century, hotspots and uncertainties from a global multimodel ensemble experiment, *Proceedings  
 968 of the National Academy of Sciences*, 111(9), 3262–3267, 2014.

969 Rakovec, O., Kumar, R., Attinger, S., and Samaniego, L.: Improving the realism of hydrologic model functioning through  
 970 multivariate parameter estimation, *Water Resour. Res.*, 52(10), 7779–7792, <https://doi.org/10.1002/2016WR019430>,  
 971 2016.

972 Riegger, J., and Tourian, M. J.: Characterization of runoff-storage relationships by satellite gravimetry and remote  
 973 sensing, *Water Resour. Res.*, 50, 3444–3466, <https://doi.org/10.1002/2013WR013847>, 2014.

974 Rodell, M., Beaudoin, H. K., L’Ecuyer, T. S., Olson, W. S., Famiglietti, J. S., Houser, P. R., Adler, R., Bosilovich, M.  
 975 G., Clayson, C. A., Chambers, D., Clark, E., Fetzer, E. J., Gao, X., Gu, G., Hilburn, K., Huffman, G. J., Lettenmaier,  
 976 D. P., Liu, W. T., Robertson, F. R., Schlosser, C. A., Sheffield, J. and Wood, E. F.: The observed state of the water  
 977 cycle in the early 15twenty-first century, *J. Clim.*, 28(21), 8289–8318, [https://doi.org/10.1175/JCLI-D-14-  
 978 00555.1](https://doi.org/10.1175/JCLI-D-14-00555.1), 2015.

979 Schellekens, J., Dutra, E., Martínez-de la Torre, A., Balsamo, G., van Dijk, A., Sperna Weiland, F., Minvielle, M., Cal-  
 980 vet, J.-C., Decharme, B., Eisner, S., Fink, G., Flörke, M., Peßenteiner, S., van Beek, R., Polcher, J., Beck, H., Orth, R.,  
 981 Calton, B., Burke, S., Dorigo, W., and Weedon, G. P.: A global water resources ensemble of hydrological models: the  
 982 earth2Observe Tier-1 dataset, *Earth Syst. Sci. Data*, 9, 389–413, <https://doi.org/10.5194/essd-9-389-2017>, 2017.



983 Schwanghart, W., and Kuhn, N. J.: TopoToolbox: A set of Matlab functions for topographic analysis., Environ. Model.  
 984 Softw.Environmental Modelling & Software, 25(6), 770-781, 2010.

985 Seneviratne, S. I., Corti, T., Davin, E. L., Hirschi, M., Jaeger, E. B., Lehner, I., ... and Teuling, A. J.: Investigating soil  
 986 moisture–climate interactions in a changing climate: A review, Earth-Sci. Rev., 99(3-4), 125-161,  
 987 <https://doi.org/10.1016/j.earscirev.2010.02.004>, 2010.

988 Sneeuw, N., Lorenz, C., Devaraju, B., Tourian, M. J., Riegger, J., Kunstmann, H., and Bárdossy, A.: Estimating runoff  
 989 using hydro-geodetic approaches, Surv. Geophys, 35(6), 1333-1359, <https://doi.org/10.1007/s10712-014-9300-4>,  
 990 2014.

991 Sobol, I.M. (1993), Sensitivity analysis for non-linear mathematical models, Math. Model. Comput. Exp. Transl. Russ.  
 992 IM Sobol' Sensit. Estim. Nonlinear Math. Models Mat. Model. 2, 1 (4) (1993), pp. 407-414, 1990 112–118.

993 Solomatine, D. P., and Ostfeld, A.: Data-driven modelling: some past experiences and new approaches, J. Hydroinform.,  
 994 10(1), 3-22, <https://doi.org/10.2166/hydro.2008.015>, 2008.

995 Sood, A., and Smakhtin, V.: Global hydrological models: a review, Hydrol. Sci. J., 60(4), 549-565,  
 996 <https://doi.org/10.1080/02626667.2014.950580>, 2015.

997 Strahler, A. N.: Hypsometric (area-altitude) analysis of erosional topography, Geol. Soc. Am. Bull.Geological Society of  
 998 America Bulletin, 63(11), 1117-1142, [https://doi.org/10.1130/0016-7606\(1952\)63\[1117:HAAOET\]2.0.CO;2](https://doi.org/10.1130/0016-7606(1952)63[1117:HAAOET]2.0.CO;2), 1952.

999 Tang, Y., Reed, P., Wagener, T. and Van Werkhoven, K. Comparing sensitivity analysis methods to advance lumped  
 1000 watershed model identification and evaluation. Hydrology & Earth System Sciences 11, 793–817, 2007.

1001 Tapley, B.D., Watkins, M.M., Flechtner, F. et al.: Contributions of GRACE to understanding climate change, Nat. Clim.  
 1002 Chang., 9, 358–369, <https://doi.org/doi:10.1038/s41558-019-0456-2>, 2019.

1003 Thiemi, V., Rojas, R., Zambrano-Bigiarini, M., and De Roo, A.: Hydrological evaluation of satellite rainfall estimates  
 1004 over the Volta and Baro-Akobo Basin, J. Hydrol., 499, 324-338, <https://doi.org/10.1016/j.jhydrol.2013.07.012>, 2013.

1005 Thornthwaite C.W., 1948. An approach toward a rational classification of climate. Geogr. Rev., 38, 55-94.

1006 Tourian, M. J., Reager, J. T., and Sneeuw, N.: The total drainable water storage of the Amazon river basin: A first estimate  
 1007 using GRACE, Water Resour. Res., 54., <https://doi.org/10.1029/2017WR021674>, 2018.

1008 Trambly, Y., Bouvier, C., Martin, C., Didon-Lescot, J. F., Todorovik, D., and Domergue, J. M.: Assessment of initial  
 1009 soil moisture conditions for event-based rainfall–runoff modelling, J. Hydrol., 387(3-4), 176-187,  
 1010 <https://doi.org/10.1016/j.jhydrol.2010.04.006>, 2010.

1011 Troutman, B. M., and Karlinger, M.B.: Unit hydrograph approximation assuming linear flow through topologically  
 1012 random channel networks, Water Resour. Res., 21., 743 – 754, <https://doi.org/doi:10.1029/WR021i005p00743>, 1985.

1013 Van Beek, L. P. H., and Bierkens, M. F. P.: The global hydrological model PCR-GLOBWB: conceptualization,  
 1014 parameterization and verification. Utrecht University, Utrecht, The Netherlands, 1, 25-26, 2009.

1015 Vishwakarma, B. D., Devaraju, B., and Sneeuw, N.: What is the spatial resolution of GRACE satellite products for  
 1016 hydrology?, Remote Sensing, 10, 852, <https://doi.org/10.3390/rs10000852>, 2018.

1017 Vörösmarty C. J., and Coauthors: Global water data: A newly endangered species, Eos, Trans. Amer. Geophys. Union,  
 1018 82, 54, <https://doi.org/10.1029/01EO00031>, 2002.

1019 Vose, R.S., Applequist, S., Durre, I., Menne, M.J., Williams, C.N., Fenimore, C., Gleason, K., and Arndt, D.: Improved  
 1020 Historical Temperature and Precipitation on Time Series For U.S. Climate Divisions., J. Meteorol. and Climat.,  
 1021 53(May), 1232–1251., <https://doi.org/10.1175/JAMC-D-13-0248.1>DOI: 10.1175/JAMC-D-13-0248.1, 2014.

1022 Wagner, W., Blöschl, G., Pampaloni, P., Calvet, J. C., Bizzarri, B., Wigneron, J. P., and Kerr, Y.: Operational readiness  
 1023 of microwave remote sensing of soil moisture for hydrologic applications, Hydrol. Res., 38(1), 1-20,  
 1024 <https://doi.org/10.2166/nh.2007.029>, 2007.

1025 Wagner, W., Lemoine, G., and Rott, H.: A method for estimating soil moisture from ERS scatterometer and soil data.,  
 1026 Remote Sens. Environ.Remote Sensing of Environment, 70, 191–207, [https://doi.org/doi:10.1016/S0034-4257\(99\)00036-X](https://doi.org/doi:10.1016/S0034-4257(99)00036-X), 1999.

1028 Wang, Y. H., Broxton, P., Fang, Y., Behrangi, A., Barlage, M., Zeng, X., and Niu, G. Y.: A wet-bulb temperature-based  
 1029 rain-snow partitioning scheme improves snowpack prediction over the drier western United States, *Geophys. Res.*  
 1030 *Lett.*, 46(23), 13825-13835, <https://doi.org/10.1029/2019GL085722>, 2019.

1031 Wisser, D., Fekete, B. M., Vörösmarty, C. J., and Schumann, A. H.: Reconstructing 20th century global hydrography: a  
 1032 contribution to the Global Terrestrial Network- Hydrology (GTN-H), *Hydrol. Earth Syst. Sci.*, 14, 1–24,  
 1033 <https://doi.org/doi:10.5194/hess-14-1-2010>, 2010.

1034 Yokoo, Y., and Sivapalan, M.: Towards reconstruction of the flow duration curve: Development of a conceptual  
 1035 framework with a physical basis, *Hydrol. Earth Syst. Sci.*, 15(9), 2805–2819, [https://doi.org/10.5194/hess-15-2805-](https://doi.org/10.5194/hess-15-2805-2011)  
 1036 2011, 2011.

1037 Zhang, Y., Pan, M., Sheffield, J., Siemann, A. L., Fisher, C. K., Liang, M., ... and Zhou, T.: A Climate Data Record  
 1038 (CDR) for the global terrestrial water budget: 1984–2010, *Hydrol. Earth Syst. Sci.*, 22, 241–263,  
 1039 [https://doi.org/10.5194/hess-22-241-2018\(Online\)](https://doi.org/10.5194/hess-22-241-2018(Online)), 22(PNNL-SA-129750), 2018.

1040

1041 Table 1. Location of river discharge gauging stations over the Mississippi basins and upstream  
1042 contributing area. Bold text is used to indicate gages where the STREAM model has been calibrated.

#	River	Gage name	Latitude (°)	Longitude (°)	Upstream area (km²)	Mean annual river discharge (m³/s)	Presence of dam
1	Missouri	Bismarck, ND	-100.82	46.81	481232	633	Garrison dam
2	Missouri	Omaha, NE	-95.92	41.26	814371	914	Gavins Point Dam
3	Missouri	Kansas City, MO	-94.59	39.11	1229427	1499	---
4	<b>Missouri</b>	<b>Hermann, MO</b>	<b>-91.44</b>	<b>38.71</b>	<b>1330000</b>	<b>2326</b>	---
5	Kansas	Wamego, KS	-96.30	39.20	143054	141	Kanopolis
6	<b>Mississippi</b>	<b>Keokuk, IA</b>	<b>-91.37</b>	<b>40.39</b>	<b>282559</b>	<b>1948</b>	---
7	Rock	Near Joslin, IL	-90.18	41.56	23835	199	---
8	Mississippi	Chester, IL	-89.84	37.90	1776221	6018	---
9	Arkansas	<b>Murray Dam Near Little Rock, AR</b>	<b>-92.36</b>	<b>34.79</b>	<b>408068</b>	<b>1249</b>	---
10	<b>Mississippi</b>	<b>Vicksburg, MS</b>	<b>-90.91</b>	<b>32.32</b>	<b>2866590</b>	<b>17487</b>	---
11	<b>Ohio</b>	<b>Metropolis, ILL.</b>	<b>-88.74</b>	<b>37.15</b>	<b>496134</b>	<b>7931</b>	---

1043  
1044

1045 Table 2. Performance scores obtained over the Mississippi river gauging stations during the  
 1046 calibration and validation periods.

#	CALIBRATION PERIOD			VALIDATION PERIOD		
SCORE	<i>KGE</i> (-)	rho (-)	<i>RRMSE</i> (%)	<i>KGE</i> (-)	rho (-)	<i>RRMSE</i> (%)
GAUGING STATIONS USED FOR CALIBRATION						
10	0.78	0.78	30	0.71	0.80	40
9	0.79	0.80	66	0.21	0.90	112
6	0.80	0.80	42	0.74	0.81	48
4	0.78	0.78	45	0.73	0.76	49
11	0.80	0.81	45	0.72	0.85	51
GAUGING STATIONS NOT USED FOR CALIBRATION						
1	-3.07	0.09	131	0.43	0.45	93
2	-0.46	0.50	110	0.44	0.54	86
3	0.23	0.73	78	0.42	0.72	69
5	-1.43	0.24	361	-1.23	0.31	355
7	0.55	0.62	72	0.34	0.64	76
8	0.81	0.84	35	0.78	0.83	39

1047  
 1048



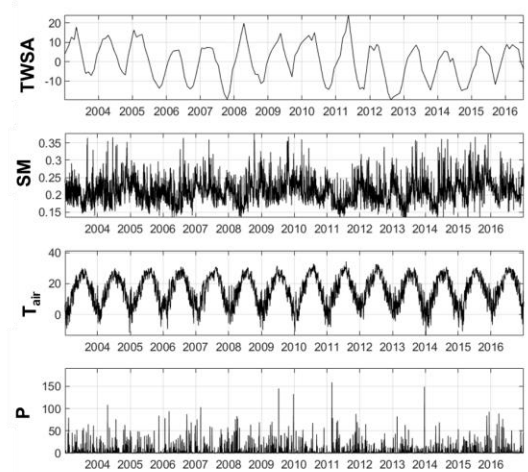
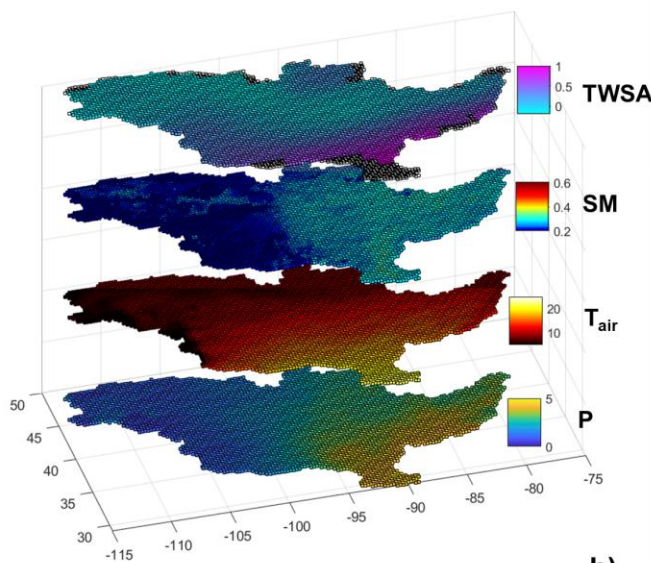
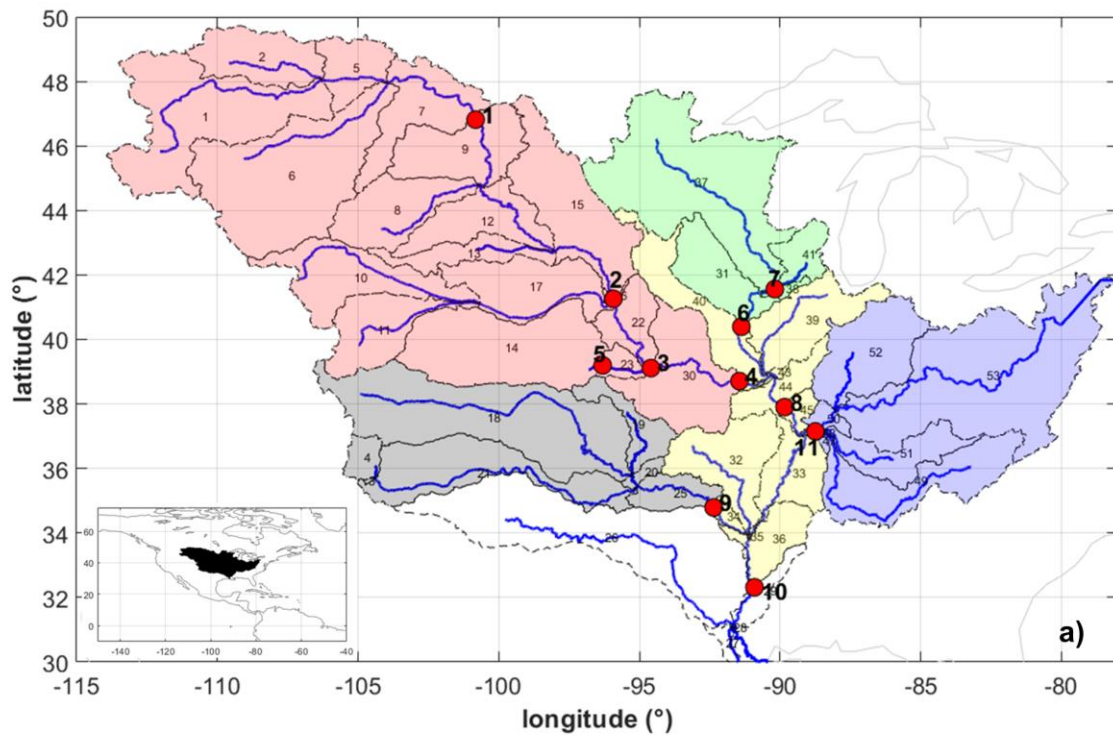


Figure 1. Mississippi river basin. Figure 1a) illustrates the sub-catchments delineation. The black dashed lines and the numbers in the map identify the 53 sub-catchments (tributary and directly draining areas) in the Mississippi basin, blue lines represent the mainstem of each sub-catchment. Red dots indicate the location of the river discharge gauging stations; different colours identify different inner cross-sections (and the related contributing sub- catchments) used for the model calibration. Figure 1b) shows the gridded mean daily values of the input data for the period 2003-2016. Figure 1c) illustrates the input time series over a point located inside the basin.

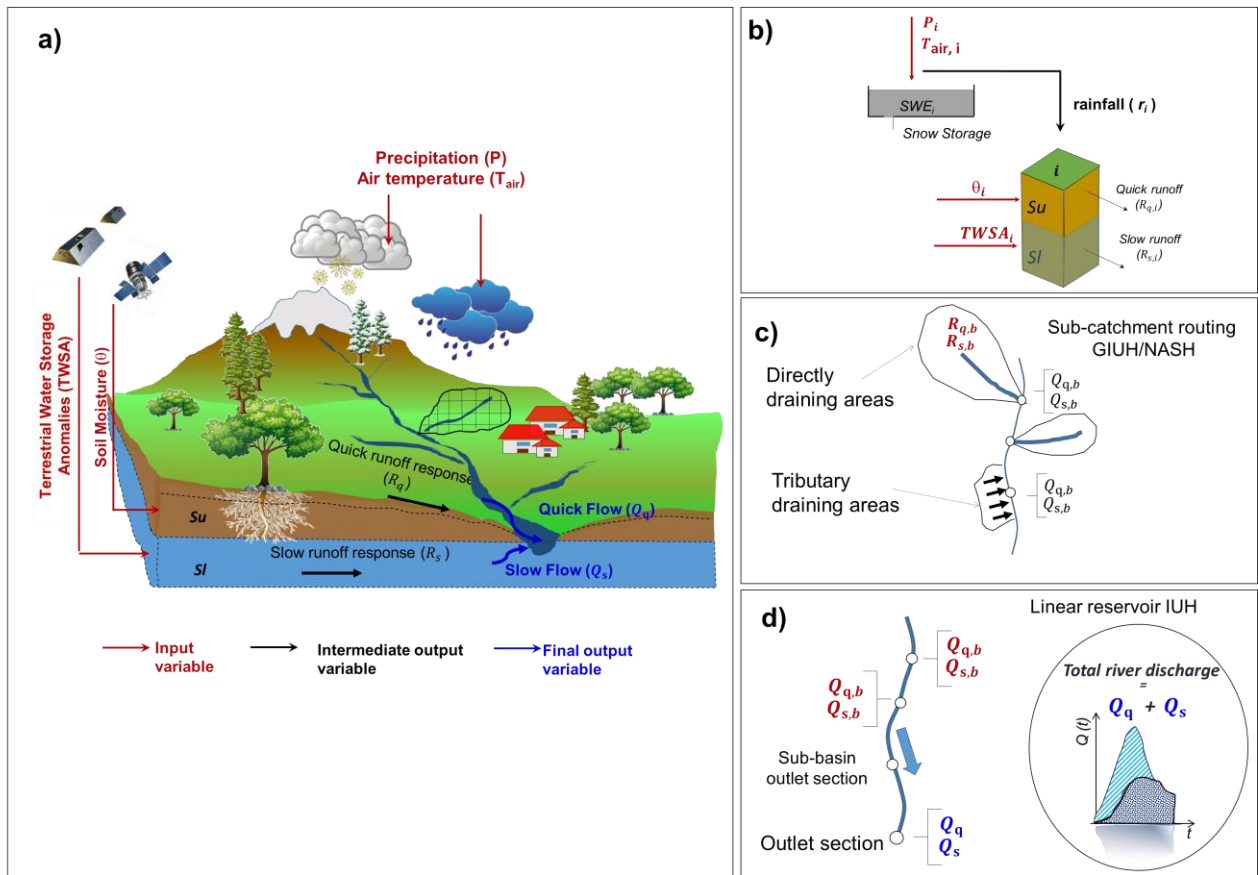
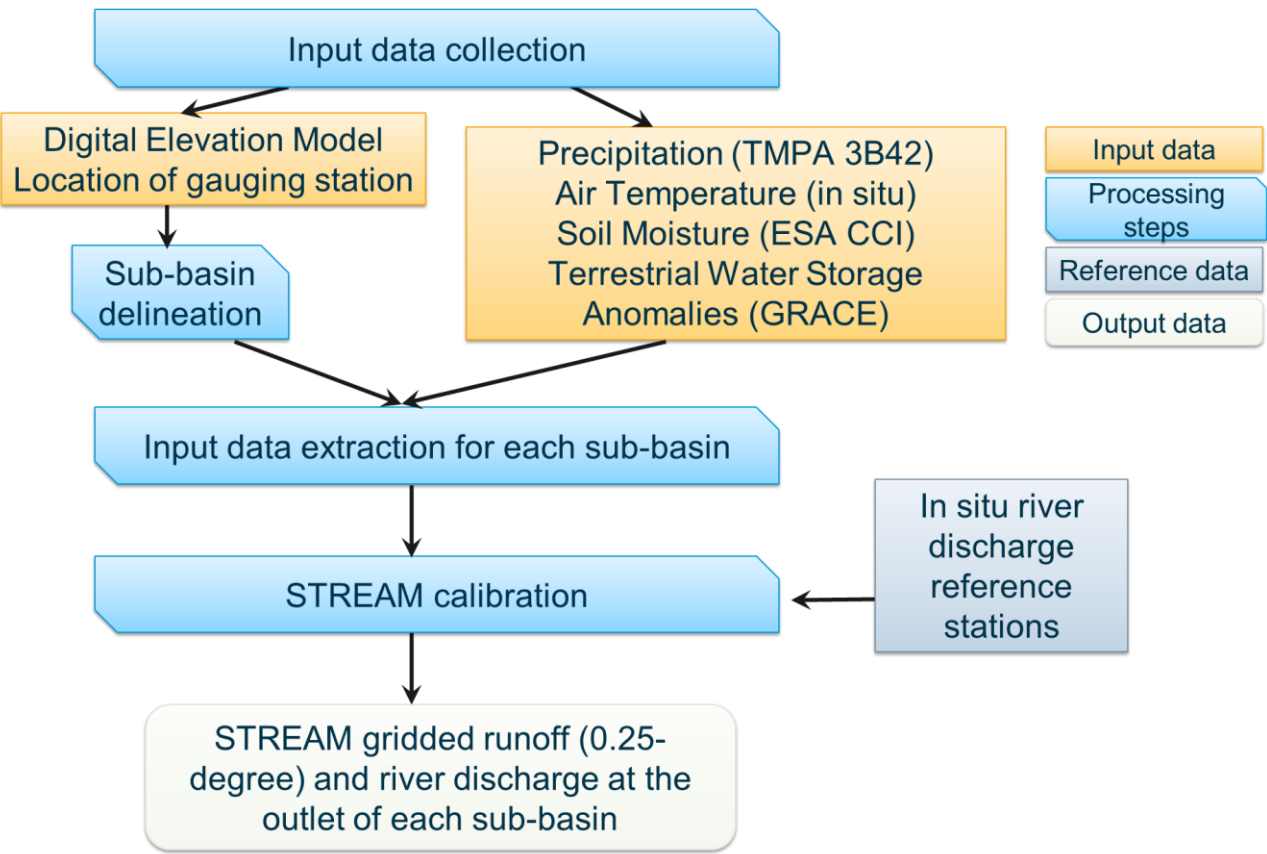


Figure 2. Configuration of the STREAM model adopted for runoff and river discharge estimation. Figure 2a) gives an overview of the needed input data and the variables can be obtained as model output. Figure 2b) illustrates the runoff generation at cell scale. Figure 2c) refers to the sub-catchment river discharge calculation and Figure 2d) illustrates the river discharge routing through river networks. Red arrows indicate input variables; black arrows indicate intermediate output variables; blue arrows indicate final output variables. Please refer to text for symbols.

1069



1070

1071

1072

1073

Figure 3. Processing steps of the STREAM model.

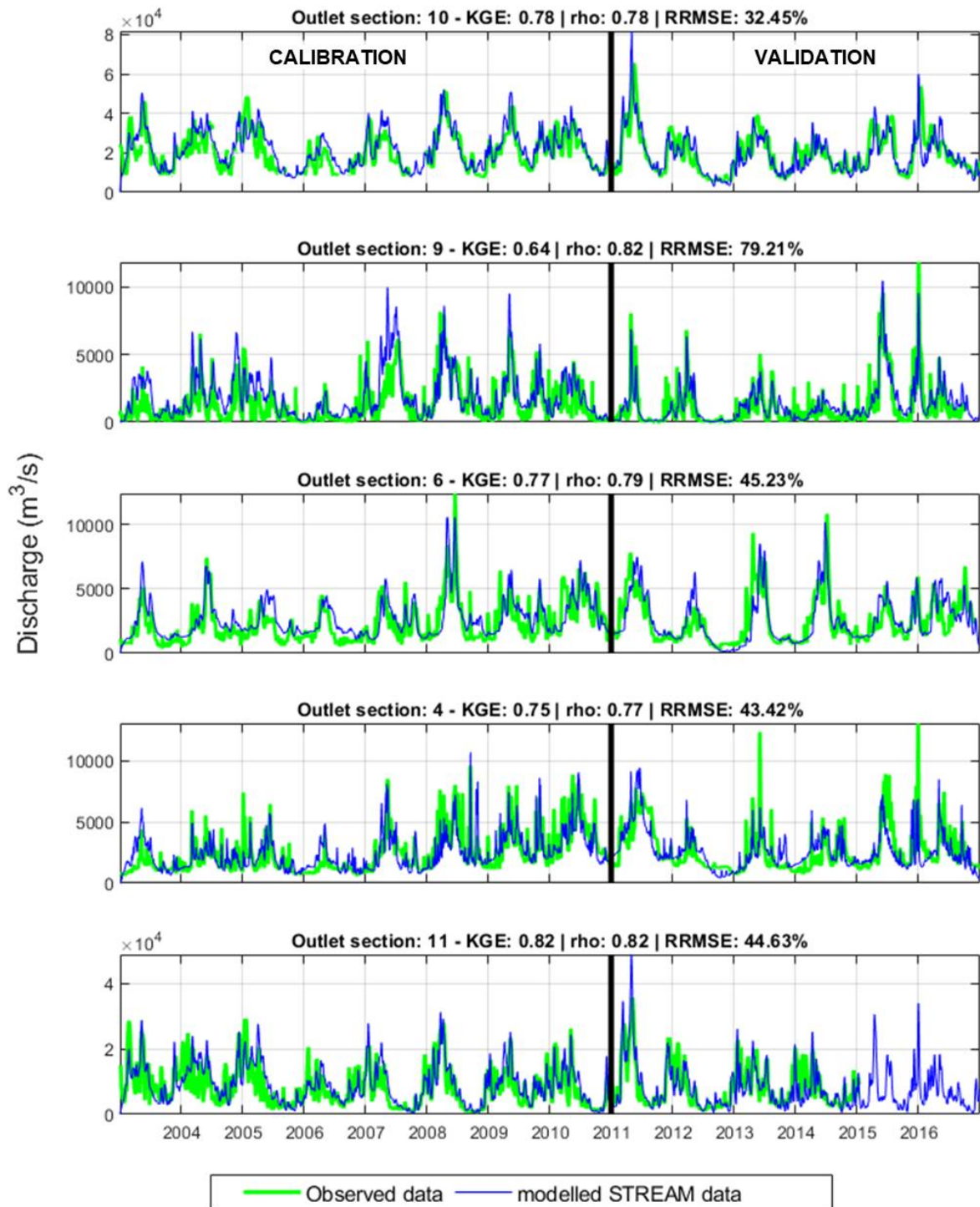


Figure 4. Comparison between observed and modelled river discharge time series over the five calibrated sections in the Mississippi river basin. Performance scores at the top of each plot refer to the entire study period (2003–2016).



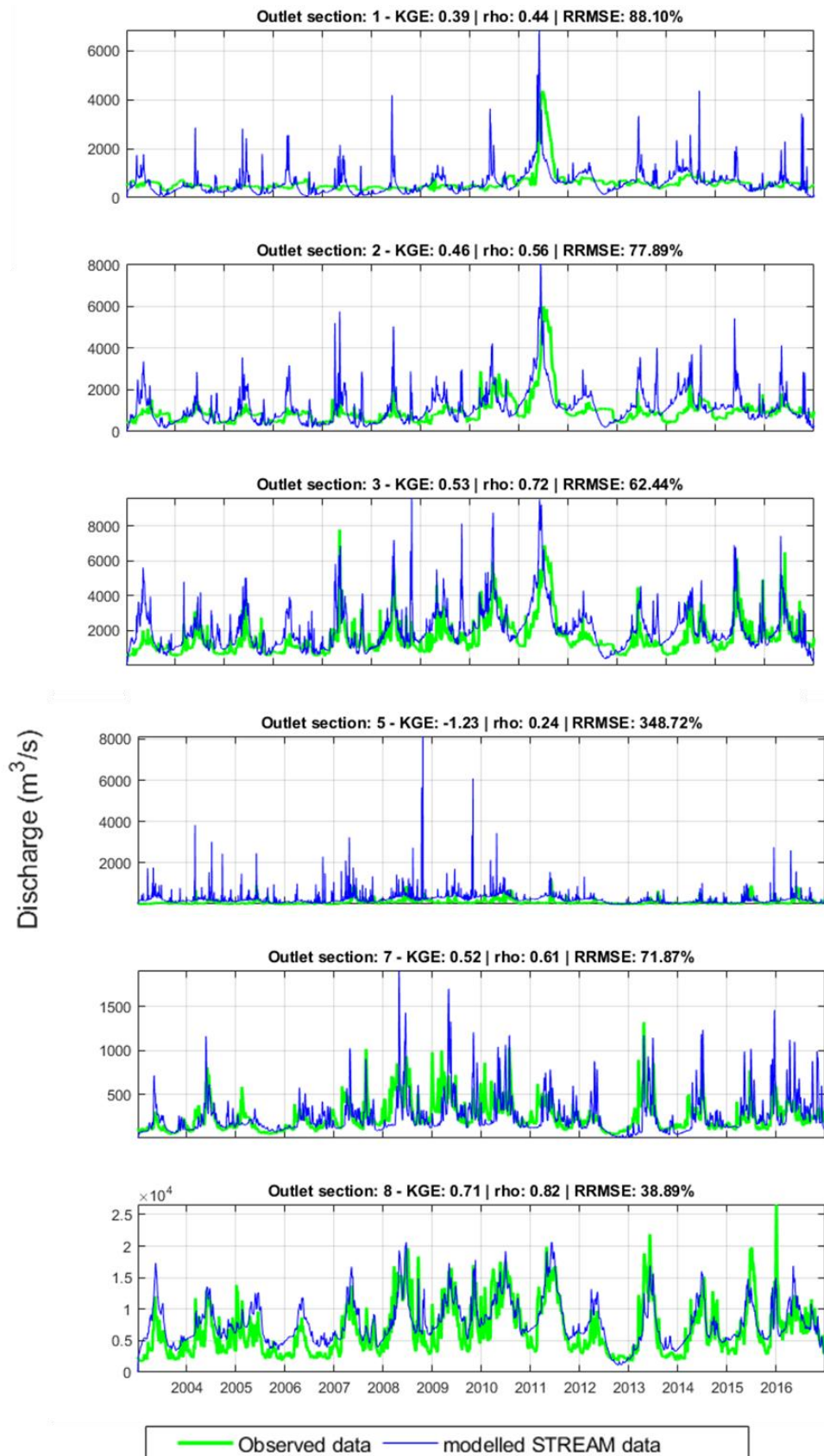
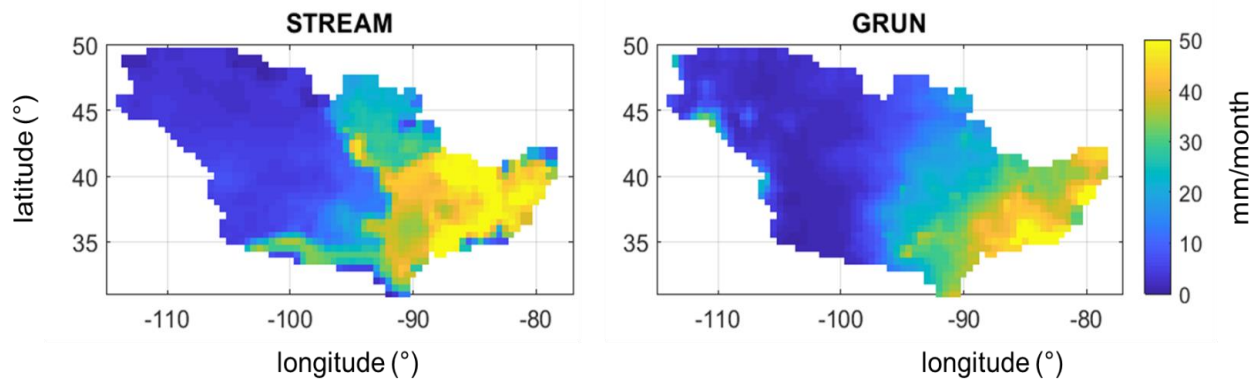


Figure 5. Comparison between observed and modelled river discharge time series over the gauged sections not used in the calibration phase. Performance scores at the top of each plot refer to the entire study period (2003–2016).



1086

1087 Figure 6. Mississippi river basin: mean monthly runoff for the period 2003–2014 obtained by  
1088 STREAM and GRUN models.

1089

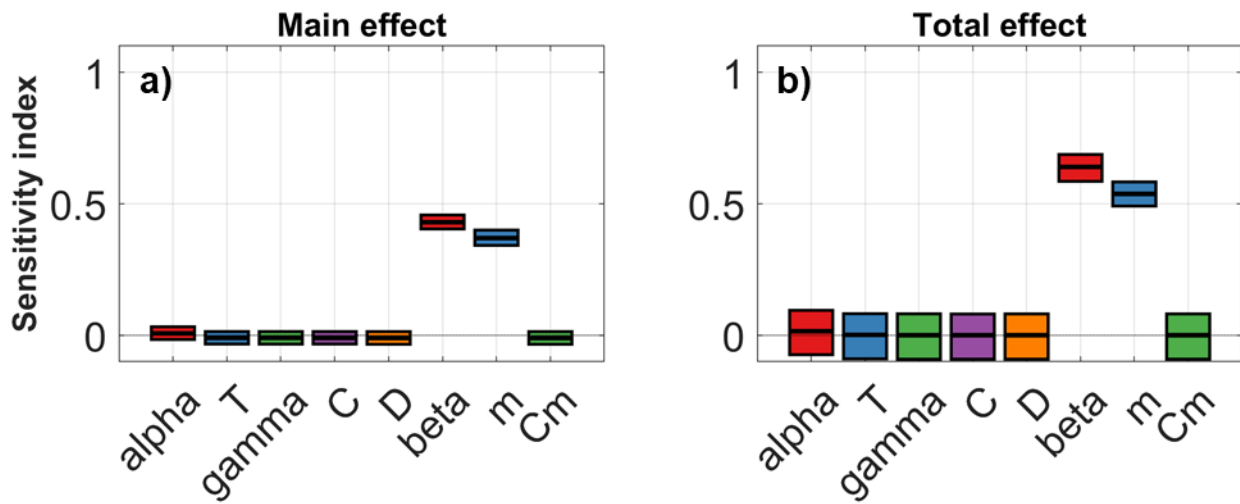


Figure 7. Main effect a) and total effect b) sensitivity indices calculated using the VBSA method for Vicksburg gauging station. The boxes represent the 95% bootstrap confidence intervals and the central black lines indicate the bootstrap mean.

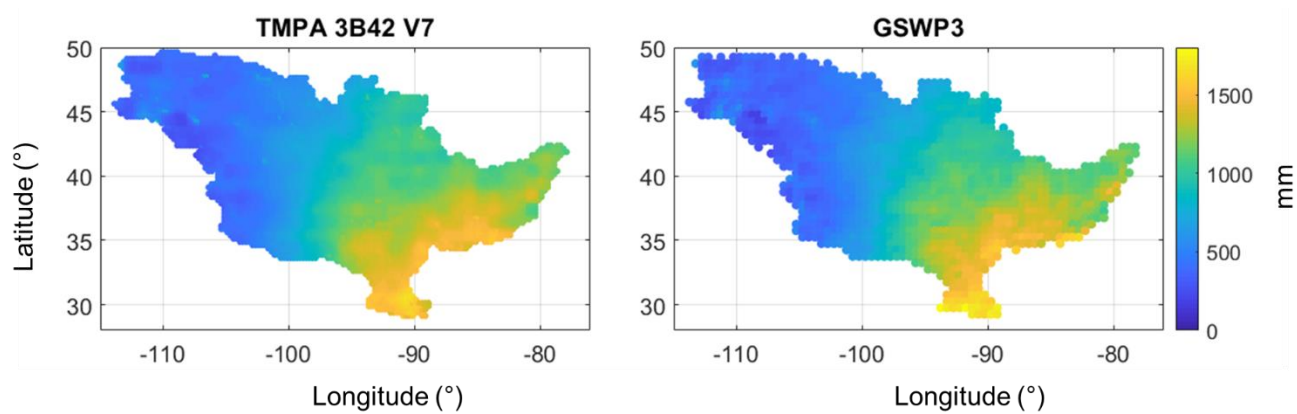
1097    Table 1A. Description of STREAM parameters, belonging module, variability range and unit.

Parameter	Description	Module	Range Variability	Unit
Cm	degree-day coefficient	Snow	0.1/24-3	[-]
$\alpha$	exponent of infiltration	Soil	1-30	[-]
T	characteristic time length	Soil	0.01-80	[days]
$\beta$	coefficient relationship <i>slow-flow</i> runoff component and TWSA	Soil	0.1-20	[mm h <sup>-1</sup> ]
m	exponent in the relationship between <i>slow-flow</i> runoff component and TWSA	Soil	1-15	[-]
$\gamma$	parameter of GIUH	Routing	0.5-5.5	[-]
C	Celerity	Routing	1-60	[km h <sup>-1</sup> ]
D	Diffusivity	Routing	1-30	[km <sup>2</sup> h <sup>-1</sup> ]

1098

1099





1100

1101 Figure S1. Mean annual precipitation data over the period 2003-2014 obtained by TMPA 3B42 V7  
 1102 and GSWP3 datasets over the Mississippi river basin.

1103